การศึกษาความสัมพันธ์ของเลขซีทีกับความหนาแน่นของอิเล็กตรอน สำหรับการคำนวณปริมาณรังสี
ที่ตำแหน่งรอยโรคบริเวณศีรษะและลำคอ ทรวงอก กระดูกสันหลัง และอุ้งเชิงกราน

นางสาวสิริพร ว่อง

วิทยานิพนธ์นี้เป็นส่วนหนึ่งของการศึกษาตามหลักสูตรปริญญาวิทยาศาสตรมหาบัณฑิต
สาขาวิชาฉายาเวชศาสตร์ ภาควิชารังสีวิทยา
คณะแพทยศาสตร์ จุฬาลงกรณ์มหาวิทยาลัย
ปีการศึกษา 2560

CT NUMBER AND ELECTRON DENSITY RELATIONSHIP FOR PHOTON DOSE CALCULATION IN HEAD AND NECK, CHEST, SPINE AND PELVIC REGIONS

Miss Siriporn Wong

A Thesis Submitted in Partial Fulfillment of the Requirements
for the Degree of Master of Science Program in Medical Imaging
Department of Radiology
Faculty of Medicine
Chulalongkorn University
Academic Year 2017

Thesis Title	CT NUMBER AND ELECTRON DENSITY RELATIONSHIP FOR PHOTON DOSE CALCULATION IN HEAD AND NECK, CHEST, SPINE AND PELVIC REGIONS
By	Miss Siriporn Wong
Field of Study	Medical Imaging
Thesis Advisor	Taweap Sanghangthum, Ph.D.

Accepted by the Faculty of Medicine, Chulalongkorn University in Partial Fulfillment of the Requirements for the Master's Degree

.....Dean of the Faculty of Medicine
(Professor Suttipong Wacharasindhu, M.D.)

THESIS COMMITTEE

.....Chairman
(Associate Professor Sivalee Suriyapee, M.Eng)

.....Thesis Advisor
(Taweap Sanghangthum, Ph.D.)

.....Examiner
(Isra Israngkul Na Ayuthaya, Ph.D.)

.....External Examiner
(Professor Franco Milano, Ph.D.)

สิริพร ว่อง : การศึกษาความสัมพันธ์ของเลขซีทีกับความหนาแน่นของอิเล็กตรอน สำหรับการคำนวณปริมาณรังสีที่ตำแหน่งรอยโรคบริเวณศีรษะและลำคอ ทรวงอก กระดูกสันหลัง และอุ้งเชิงกราน (CT NUMBER AND ELECTRON DENSITY RELATIONSHIP FOR PHOTON DOSE CALCULATION IN HEAD AND NECK, CHEST, SPINE AND PELVIC REGIONS) อ.ที่ปรึกษาวิทยานิพนธ์หลัก: อ. ดร. ทวีป แสงแห่งธรรม, 56 หน้า.

ภาพจากเครื่องเอกซเรย์คอมพิวเตอร์ให้ข้อมูลของเลขซีที ซึ่งมีความสัมพันธ์กับค่าความหนาแน่นของอิเล็กตรอน โดยค่าความหนาแน่นของอิเล็กตรอนมีส่วนสำคัญในการช่วยแก้ค่าความไม่สม่ำเสมอของเนื้อเยื่อขึ้น วัตถุประสงค์ในการทำงานวิจัยนี้คือเพื่อศึกษาผลกระทบต่อการกระจายของปริมาณรังสีในแผนการรักษาแบบสามมิติ ปรับความเข้ม และปรับความเข้มแบบหมุนรอบตัว เมื่อใช้กราฟความสัมพันธ์ของเลขซีทีกับความหนาแน่นของอิเล็กตรอนแบบเดียว แต่ทำเอกซเรย์คอมพิวเตอร์ด้วยค่าความต่างศักย์ที่แตกต่างกัน

ทำการสแกนหุ่นจำลองมนุษย์ โดยใช้เครื่องเอกซเรย์คอมพิวเตอร์จากบริษัท ซีเมนต์ รุ่น SOMATOM Definition AS ตั้งค่าความต่างศักย์ 120 กิโลวัตต์ ใช้ภาพที่ได้เป็นภาพมาตรฐานสำหรับเปรียบเทียบ จากนั้นสแกนโดยการเปลี่ยนการตั้งค่าความต่างศักย์เป็น แบบสองความต่างศักย์ (80/140 กิโลวัตต์) 80 และ 140 กิโลวัตต์ จากนั้นใช้กราฟความสัมพันธ์ระหว่างเลขซีทีกับค่าความหนาแน่นของอิเล็กตรอนที่ได้จากสแกนแฟนทอม Gammex 467 ที่ทราบค่าความหนาแน่นของอิเล็กตรอนด้วยความต่างศักย์ 120 กิโลวัตต์ ไปปรับใช้ในระบบการวางแผนการรักษาเพื่อคำนวณปริมาณรังสีที่ในทุกกลุ่มตัวอย่างที่นำมาศึกษา แผนการรักษาของผู้ป่วยจำนวน 5 รายในเทคนิคการรักษาแบบสามมิติ ปรับความเข้ม และปรับความเข้มแบบหมุนรอบตัว ใน 4 บริเวณรอยโรค (ศีรษะและลำคอ ทรวงอก กระดูกสันหลัง และอุ้งเชิงกราน) คำนวณปริมาณรังสีในแต่ละภาพเอกซเรย์คอมพิวเตอร์ที่มีการตั้งค่าความต่างศักย์ที่แตกต่างกัน นอกจากนี้มีการใส่อะมอลกัม ลงในหุ่นจำลองมนุษย์ที่บริเวณช่องปากและคำนวณปริมาณรังสีเฉพาะบริเวณศีรษะและลำคอเท่านั้น ประเมินความแตกต่างของปริมาณรังสีจากปริมาณรังสีที่จุดศูนย์กลางและค่าดัชนีแกมมาด้วยเกณฑ์ 1%/1 มม. มาใช้ประเมิน

จากการทดลองพบว่าค่าเฉลี่ยปริมาณรังสีที่จุดศูนย์กลางต่างจากค่ามาตรฐานในแต่ละบริเวณรอยโรคจากการตั้งค่าความต่างศักย์ แบบสองความต่างศักย์, 80 และ 140 กิโลวัตต์ มีค่าตามลำดับดังนี้ 0.7%, 0.4% และ 0.3% สำหรับบริเวณศีรษะและคำคอ, 0.5%, 0.3% และ 0.2% สำหรับทรวงอก, 0.6%, 0.5% และ 0.1% สำหรับกระดูกสันหลัง, 0.9%, 0.2% และ 0.2% สำหรับอุ้งเชิงกรานและ 0.1%, 0.4% และ 0.1% สำหรับกรณีที่ใส่อะมอลกัม สำหรับค่าดัชนีแกมมา อัตราการผ่านของแกมมาค่าเฉลี่ยของทุกบริเวณรอยโรคและทุกเทคนิคการรักษา ด้วยเกณฑ์ 1%/1 มม. ค่าเฉลี่ยที่ได้สำหรับภาพจากการตั้งค่าความต่างศักย์ แบบสองความต่างศักย์, 80 และ 140 กิโลวัตต์ มีค่าเท่ากับ 95.9%, 100% และ 100% ตามลำดับ

จากผลของการศึกษาพบว่า ปริมาณรังสีที่เปลี่ยนแปลงไปที่จุดศูนย์กลางแสดงให้เห็นว่าผลที่เกิดขึ้นมีแนวโน้มสอดคล้องกับผลของค่าดัชนีแกมมา โดยภาพจากการตั้งค่าความต่างศักย์แบบสองค่าจะให้ค่าเฉลี่ยปริมาณรังสีที่เปลี่ยนไปที่จุดศูนย์กลางมากที่สุด โดยเฉพาะอย่างยิ่งบริเวณที่มีความพื้นที่ของอวัยวะที่หนาแน่นสูงจำนวนมาก อย่างไรก็ตามในกรณีที่มีการใส่อะมอลกัม ค่าเฉลี่ยปริมาณรังสีที่เปลี่ยนแปลงไปมีค่าลดลง รอยโรคบริเวณอุ้งเชิงกรานให้ค่าความแตกต่างเฉลี่ยสูงที่สุดเมื่อเทียบกับรอยโรคบริเวณอื่น เนื่องจากบริเวณนี้ประกอบไปด้วยอวัยวะที่มีความหนาแน่นสูง เช่น กระดูกอุ้งเชิงกราน เป็นต้น เมื่อเปรียบเทียบผลศึกษาผลในแต่ละเทคนิคการรักษา พบว่าเทคนิคการรักษาแบบปรับความเข้มและปรับความเข้มแบบหมุนรอบตัว เป็นเทคนิคที่มีค่าความแตกต่างเฉลี่ยสูงที่สุด เนื่องมาจากเป็นเทคนิคที่มีค่ามอนิเตอร์ยูนิตที่สูงและมีการเคลื่อนที่ของวัสดุกำบังรังสีที่ซับซ้อน

ผลจากการศึกษาในครั้งนี้พบว่าการใช้กราฟความพันธ์เพียงแบบเดียว สำหรับทุกการตั้งค่าความต่างศักย์สามารถเป็นไปได้ ด้วยผลของค่าเฉลี่ยปริมาณรังสีที่แตกต่างไม่เกิน 0.6% และค่าเฉลี่ยอัตราการผ่านของดัชนีแกมมาด้วยเกณฑ์ 1%/1 มม. มีค่ามากกว่า 95.9%

ภาควิชา รังสีวิทยา ลายมือชื่อนิสิต .....

สาขาวิชา ฉายาเวชศาสตร์ ลายมือชื่อ อ.ที่ปรึกษาหลัก .....

ปีการศึกษา 2560

5974046330 : MAJOR MEDICAL IMAGING
KEYWORDS: CT SIMULATOR / DECT / CT NUMBER AND ELECTRON DENSITY / GAMMA INDEX

SIRIPORN WONG: CT NUMBER AND ELECTRON DENSITY RELATIONSHIP FOR PHOTON DOSE CALCULATION IN HEAD AND NECK, CHEST, SPINE AND PELVIC REGIONS. ADVISOR: TAWEAP SANGHANGTHUM, Ph.D., 56 pp.

CT images supply the HU information that relates to electron density (ρ_e). The ρ_e is important for tissue inhomogeneity correction for accurate dose calculation. The purpose of this study was to evaluate the dosimetric effect on CT images on different kVp setting using single HU-ρ_e curve.

Anthropomorphic phantom was scanned using Siemens-SOMATOM Definition AS with 120 kVp setting and used as a reference image set. The procedures were repeated with DECT option (80/140 kVp), 80 and 140 kVp. The 120 kVp HU-ρ_e relationship curve from Gammex 467 tissue characterization phantom was created and applied into Eclipse treatment planning system. The five clinical plans in each 3D, IMRT and VMAT techniques in four regions (head and neck, chest, spine and pelvic regions) were exported and recalculated in Anthropomorphic phantom images for all kVp setting images. Moreover, the amalgam was inserted in Anthropomorphic phantom at teeth location and the radiation dose in head and neck region was evaluated. The isocenter dose and gamma index from SNC patient software with criteria 1%/1mm. ($\gamma_{1\%/1mm.}$) were selected for plan evaluation.

According to treatment regions, the average point dose differences of DECT, 80 and 140 kVp images to reference image were 0.7%, 0.4% and 0.3% for H&N, 0.5%, 0.3% and 0.2% for chest, 0.6%, 0.5% and 0.1% for spine, 0.9%, 0.2% and 0.2% for pelvic region and 0.1%, 0.4% and 0.1% for H&N with amalgam, respectively. For gamma index, the average $\gamma_{1\%/1mm.}$ passing rate in all regions and all techniques of DECT, 80 and 140 kVp images were 95.9%, 100% and 100%, respectively.

From the results, the different kVp images gave the different HU value and it has impacted to dose distribution. The results of isocenter dose differences showed the good agreement with gamma index results. DECT images presented the highest average dose differences from other energies, especially in large area of high density. Pelvic region displayed the highest average dose differences than other regions because it consists of the large bone area in pelvic bone. IMRT and VMAT technique showed the highest average dose difference that might be due to the high MU and complicated leaf movements.

In conclusion, it is possible to apply single 120 kVp HU-ρ_e relationship curve into all tube voltage scanning images with the highest average point dose difference of 0.6% in DECT and lowest average $\gamma_{1\%/1mm.}$ passing rate of 95.9%.

Department: Radiology Student's Signature .....
Field of Study: Medical Imaging Advisor's Signature .....
Academic Year: 2017

ACKNOWLEDGEMENTS

Foremost, I express deep and sincere gratitude to my advisor Mr. Taweap Sanghangthum, Ph.D., Division of Radiation Oncology, Department of Radiology, Faculty of Medicine, Chulalongkorn University for his patience, motivation, enthusiasm, immense knowledge and continuous support of me to perform this research. His guidance helped me in all the time of research and writing of this thesis. I could not have imagined having a better advisor.

I would like to express my sincere appreciation to Associate Professor Sivalee Suriyapee, M.Eng, Division of Radiation Oncology, Department of Radiology, Faculty of Medicine, Chulalongkorn University, who is the chairman of the thesis defense for her encouragement, kind suggestions, insightful comments and shareable her knowledge.

I acknowledge with thanks the kind of patronage and good inspiration, which I have received from Mr. Sornjarod Oonsiri, Division of Radiation Oncology, King Chulalongkorn Memorial Hospital.

I would like to thank Mr. Tanawat Tawonwong, Mrs. Puntiwa Oonsiri, Miss Chotika Jampangern, Mr. Jaruek Kanphet and all of the staff in Division of Radiation Oncology, King Chulalongkorn Memorial Hospital for sharing their ideas, giving many good advices.

I am very much thankful to Associate Professor Anchali Krisanachinda, Ph.D., Division of Nuclear Medicine, Department of Radiology, Faculty of Medicine, Chulalongkorn University for her generous suggestion and encouragement.

I would like to thank all lecturers and staff in the Master of Science Program in Medical Imaging, Faculty of Medicine, Chulalongkorn University for their teaching in Medical Imaging.

I would like to thank Mr. Isra Israngkul Na Ayuthaya, Ph.D., Division of Radiation Oncology, King Chulalongkorn Memorial Hospital, who is the examiner of the thesis defense for his help, valuable suggestions and comments in this research.

I would like to thank Professor Franco Milano, Ph.D., who is the external examiner of the thesis defense for kind suggestions and comments in this research.

I would like to thank my classmates (MICU14) for their help, valuable comments and shareable their knowledge.

Last but not the least I would like to thank my parents, my sister and my close friends for their invaluable encouragement, care, moral support and understanding during the entire of the study.

CONTENTS

Page

Page

LIST OF TABLES

Table **Page**

LIST OF FIGURES

Figure **Page**

Figure Page

LIST OF ABBREVIATIONS

Abbreviations	Terms
3D-CRT	Three dimension conformal radiation therapy
ρ_e	Electron density
AEC	Automatic exposure control
CBCT	Cone beam computed tomography
CT	Computed tomography
DECT	Dual energy computed tomography
DRR	Digital reconstructed radiograph
DVH	Dose volume histogram
E	Energy
EDP	Electron density phantom
HU	Hounsfield unit
IGRT	Image guided radiotherapy
IMRT	Intensity modulated radiation therapy
kVp	Kilo voltage peak
MU	Monitor unit
PDD	Percentage depth dose
PTV	Planning target volume
QA	Quality assurance
ROI	Region of interest
SRS	Stereotactic radiosurgery
TPS	Treatment planning system
VMAT	Volumetric modulated arc therapy
Z	Atomic number

CHAPTER I

INTRODUCTION

1.1 Introduction

Computed tomography (CT) scan is the most common diagnostic equipment used for treatment planning in external beam radiation therapy. In addition, CT scan is considered as the gold standard to acquire images due to its ability to provide an accurate geometry, good information of bone definition, and supplies the CT number information in terms of Hounsfield unit (HU). The HU values are related to electron density (ρ_e) values (1). The ρ_e is very important for tissue inhomogeneity correction in treatment planning system to obtain an accurate dose calculation of MV energy range based on Compton interaction. According to this reason, the HU-ρ_e relationship curve is created and incorporated to the treatment planning system (TPS) to convert HU values to ρ_e values for dose calculation. The value of HU depends on the quality of x-ray beams and the values can be different among several scanners. Even in a single scanner, HU in the similar tissue depends on the kVp setting and beam filtration (2).

Dual energy CT (DECT) scanners are nowadays available as a simulation machine in radiotherapy field. It involves the acquisition of CT datasets from two different x-ray spectra. For the clinical purpose, it is used for normal tissue characterization, improving dose calculation accuracy of brachytherapy and proton therapy, and reducing metal artifact (3).

The difference between CT number and electron density relationship (HU-ρ_e) will be affecting the calculated dose. Research conducted by Rhee D.J. et al.(4) showed the dose calculation error in percentage depth dose (PDD) of electron density conversion curve between 80 kVp and 140 kVp. In the clinical case, the different between CT number and electron density conversion curves of 80 kVp and 140 kVp was applied to the same image and the result showed maximum difference of 1.1% at the central region of the phantom.

At the Division of Radiation Oncology, King Chulalongkorn Memorial Hospital, the data for HU-ρ_e relationship was obtained only from CT scan under tube voltage of 120 kVp. However, the new CT-simulator in our center has various kVp setting and multiple options of DECT scan under different tube voltage. The possibility to use single HU-ρ_e relationship data to different tube voltage setting for inhomogeneity correction in TPS would be beneficial.

Therefore, in this study, the effects of CT image during scanning under different tube voltage using single 120 kVp HU-ρ_e relationship curve were studied for calculation of the radiation dose in head and neck, chest, spine, and pelvic regions.

1.2 Research objective

To evaluate the dosimetric effects on different kVp CT images using single HU-ρ_e relationship curve in head and neck, chest, spine and pelvic regions.

1.3 Definitions

1.3.1 CT number

CT number is the number used to represent the mean x-ray attenuation associated with each elemental area of CT image. CT numbers are normally expressed in terms of Hounsfield units (HU). Measured values of attenuation are transformed into CT number using the international Hounsfield scale:

$$CT\ number = \left[\frac{\mu_{tissue} - \mu_{water}}{\mu_{water}}\right] \times 1000 \quad \text{(HU)}$$

where μ is the effective linear attenuation coefficient of the x-ray beam.

1.3.2 HU-ρ_e relationship curve

HU-ρ_e relationship curve is the curve that represents the relationship between mean measured CT number value (HU) of various materials in electron density phantom and relative electron density value.

CHAPTER II

REVIEW OF RELATED LITERATURES

2.1 Theories

2.1.1 Photon interaction (5)

X-ray photons are created by the interaction of energetic electrons with matter at the atomic level. Photons (x-ray and gamma) end their lives by transferring their energy to electrons contained in matter.

Photons are individual units of energy. As an x-ray beam or gamma radiation passes through an object, three possible fates await each photon, as shown in fig.2.1:

1. It can penetrate the section of matter without interacting.
2. It can interact with the matter and be completely absorbed by depositing its energy.
3. It can interact and be scattered or deflected from its original direction and deposit part of its energy.

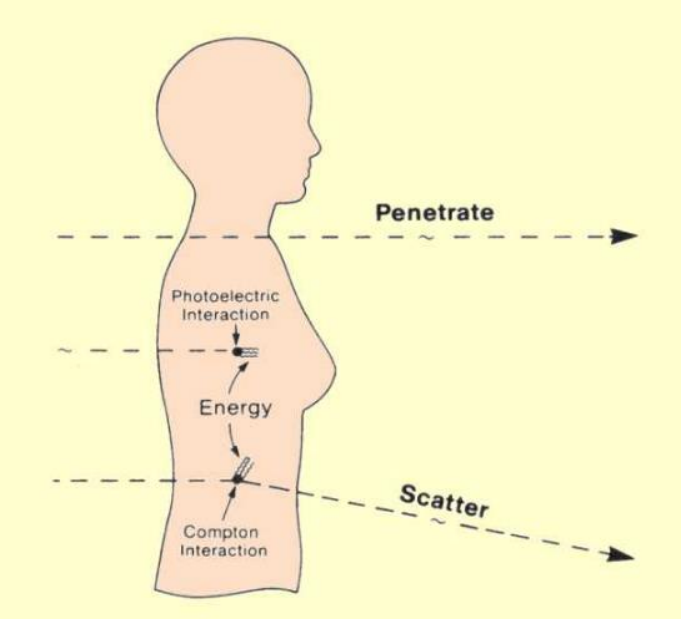

Figure 2.1 Three possible fates await each photon when photons entering the human body.

There are three main kinds of photon interactions:

2.1.1.1 Photoelectric

In the photoelectric (photon-electron) interaction, a photon transfers all its energy to an electron located in one of the atomic shells, as shown in fig.2.2. The electron is ejected from the atom by this energy and begins to pass through the surrounding matter. The electron rapidly loses its energy and moves only a relatively short distance from its original location. The photon's energy is, therefore, deposited in the matter close to the site of the photoelectric interaction. The energy transfer is a two-step process. The photoelectric interaction in which the photon transfers its energy to the electron is the first step. The depositing of the energy in the surrounding matter by the electron is the second step.

Photoelectric interactions usually occur with electrons that are firmly bound to the atom, that is, those with a relatively high binding energy. Photoelectric interactions are most probable when the electron binding energy is only slightly less than the energy of the photon. If the binding energy is more than the energy of the photon, a photoelectric interaction cannot occur. This interaction is possible only when the photon has sufficient energy to overcome the binding energy and remove the electron from the atom.

The photon's energy is divided into two parts by the interaction. A portion of the energy is used to overcome the electron's binding energy and to remove it from the atom. The remaining energy is transferred to the electron as kinetic energy and is deposited near the interaction site. Since the interaction creates a vacancy in one of the electron shells, typically the K or L, an electron moves down to fill in. The drop in energy of the filling electron often produces a characteristic x-ray photon. The energy of the characteristic radiation depends on the binding energy of the electrons involved. Characteristic radiation initiated by an incoming photon is referred to as fluorescent radiation. Fluorescence, in general, is a process in which some of the energy of a photon is used to create a second photon of less energy. This process sometimes converts x-rays into light photons. Whether the fluorescent radiation is in the form of light or x-rays depends on the binding energy levels in the absorbing material.

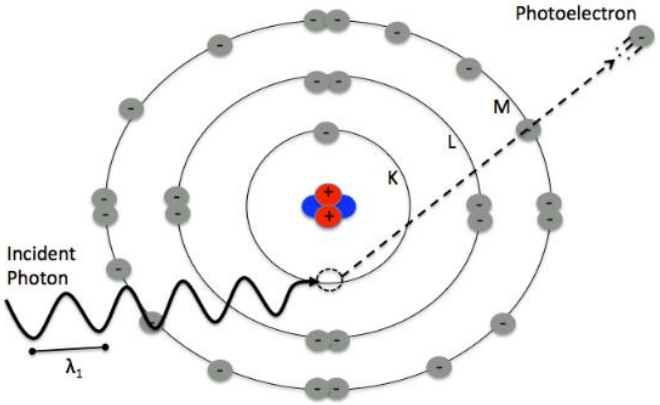

Figure 2.2 Photoelectric interaction

The probability, and thus attenuation coefficient value, for photoelectric interactions depends on how well the photon energies and electron binding energies match, as shown in fig.2.3. This can be considered from two perspectives.

In a specific material with a fixed binding energy, a change in photon energy alters the match and the chance for photoelectric interactions. On the other hand, with photons of a specific energy, the probability of photoelectric interactions is affected by the atomic number of the material, which changes the binding energy.

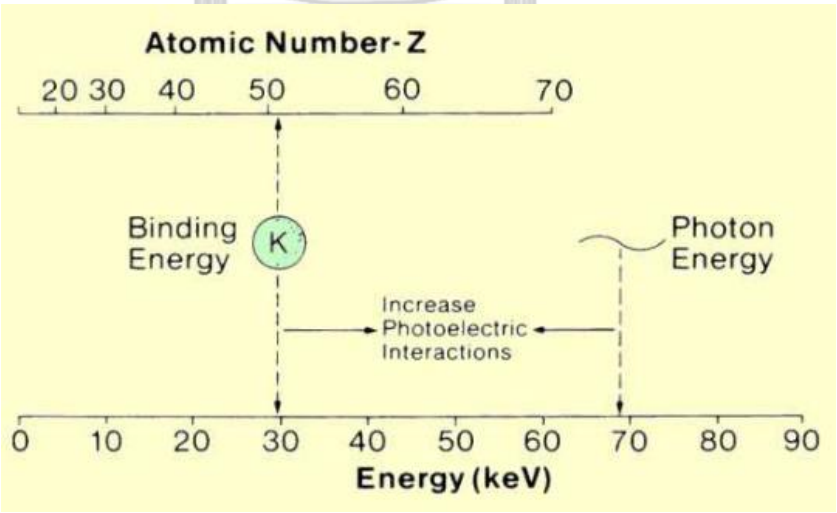

Figure 2.3 Relationship between material atomic number and photon energy that enhances the probability of photoelectric interactions.

Dependence on photon energy

In a given material, the probability of photoelectric interactions occurring is strongly dependent on the energy of the photon and its relationship to the binding energy of the electrons. The probability of photoelectric interactions is inversely proportional to the cube of the photon energy ($1/E^3$). This general relationship can be used to compare the photoelectric attenuation coefficients at two different photon energies. The significant point is that the probability of photoelectric interactions occurring in a given material drops drastically as the photon energy is increased.

Dependence on material atomic number

The probability of photoelectric interactions occurring is also dependent on the atomic number of the material. An explanation for the increase in photoelectric interactions with atomic number is that as atomic number is increased, the binding energies move closer to the photon energy. The general relationship is that the probability of photoelectric interactions (attenuation coefficient value) is proportional to Z^3. In general, the conditions that increase the probability of photoelectric interactions are low photon energies and high-atomic-number materials.

2.1.1.2 Compton or Incoherent scattering

A Compton interaction is one in which only a portion of the energy is absorbed and a photon is produced with reduced energy, as shown in fig.2.4. This photon leaves the site of the interaction in a direction different from that of the original photon, as shown in the previous figure. Because of the change in photon direction, this type of interaction is classified as a scattering process. In effect, a portion of the incident radiation "bounces off' or is scattered by the material. This is significant in some situations because the material within the primary x-ray beam becomes a secondary radiation source. The most significant object producing scattered radiation in an x-ray procedure is the patient's body. The portion of the patient's body that is within the primary x-ray beam becomes the actual source of scattered radiation. This has two undesirable consequences. The scattered radiation that continues in the forward, direction and reaches the image receptor decreases the quality (contrast) of the image.

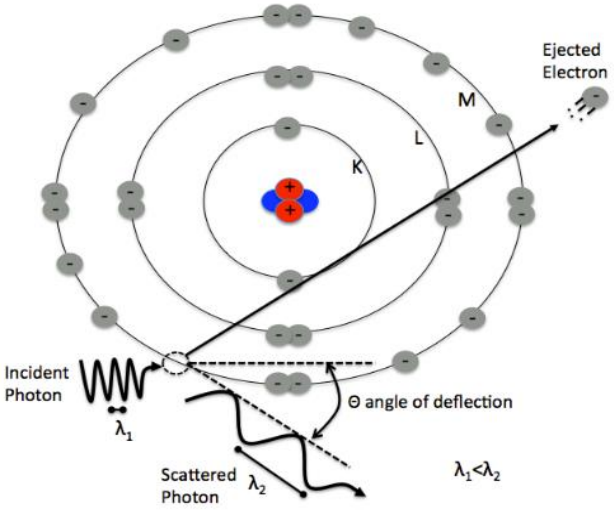

Figure 2.4 Compton interaction

Compton interactions can occur with the very loosely bound electrons. All electrons in low-atomic-number materials and the majority of electrons in high-atomic-number materials are in this category. The characteristic of the material that affects the probability of Compton interactions is the number of available electrons. Since the concentration of electrons in a given volume is proportional to the density of the materials, the probability of Compton interactions is proportional only to the physical density and not to the atomic number, as in the case of photoelectric interactions. The major exception is in materials with a significant proportion of hydrogen. In these materials with more electrons per gram, the probability of Compton interactions is enhanced.

Although the chances of Compton interactions decrease slightly with photon energy, the change is not rapid as for photoelectric interactions, which are inversely related to the cube of the photon energy.

Direction of scatter

It is possible for photons to scatter in any direction. The direction in which an individual photon will scatter is purely a matter of chance. There is no way in which the angle of scatter for a specific photon can be predicted. However, there are certain directions that are more probable and that will occur with a greater frequency than others. The factor that can alter the overall scatter direction pattern is the energy of the original photon. In diagnostic examinations, the most significant scatter will be in the forward direction. This would be an angle of scatter of only a few degrees. However, especially at the lower end of the energy spectrum, there is a significant amount of scatter in the reverse direction, i.e., backscatter. For the diagnostic photon energy range, the number of photons that scatter at right angles to the primary beam is in the range of one-third to one-half of the number that scatter in

the forward direction. Increasing primary photon energy causes a general shift of scatter to the forward direction. However, in diagnostic procedures, there is always a significant amount of back- and side-scatter radiation

2.1.1.3 Pair production

Pair production occurs when a photon passes very close to the nucleus of an atom, as shown in fig.2.7. If the energy of the photon is high enough, the photon may disappear and 'create' an electron and a positron. The new particles move away with the remaining energy of the photon converted to kinetic energy. The positron will typically annihilate once it loses its kinetic energy, giving rise to annihilation quanta (two photons with energy of 0.511 keV).

Pair production only occurs when photon energy is high enough and when there is an object of sufficient mass to take on the momentum gained by the new particles.

- Photon energy must be at least 1.022 MeV to generate a positron/electron pair. This is because 1.022 MeV is required to create the mass of the electron and the positron (through $E=mc^2$).
- Pair production only occurs in close proximity to the nucleus. This is so momentum of the electron and positron is conserved.
    - It is possible for pair production to occur in proximity to an electron. This is called triplet production, below.

Pair production does not occur with photon energy less than 1.022 MeV. Once this threshold is reached, it becomes more likely as photon energy increases. Pair production is related to the atomic number of a material through Z^2.

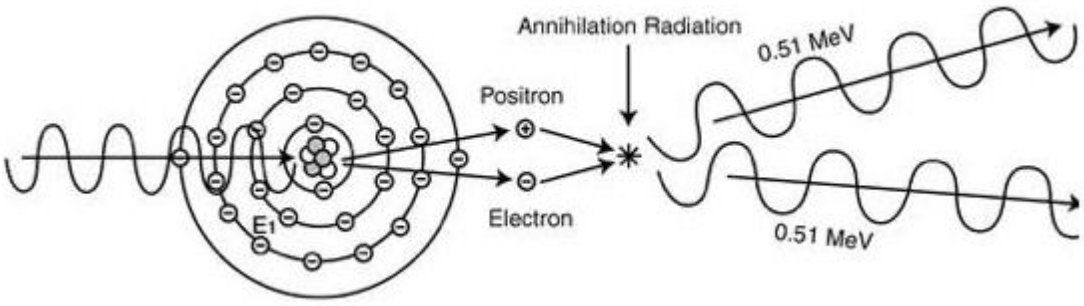

Figure 2.5 Pair production interaction

Photon interactions with tissue, such as photo-electric absorption, compton scatter, and pair production, are dependent on the atomic number, electron density of the tissue, and photon energy, as shown in fig 2.6. Therefore, to accurately calculate the radiation dose, the specific mass attenuation factor for different types of tissue, that is, heterogeneity, encountered by a photon beam must be identified. For this reason the treatment planning dose calculation is still only possible using CT.

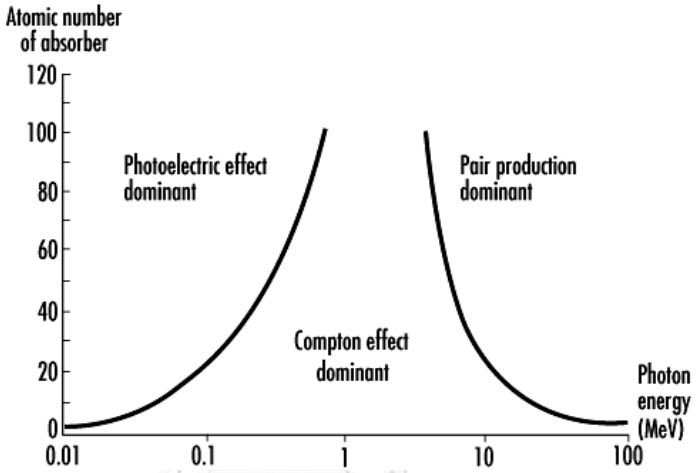

Figure 2.6 Relative of the three importance principal interactions of photons in matter

2.1.2 Computed tomography (CT)

A computed tomography (CT) scan (fig.2.7) is the special X-ray tests that produce cross-sectional images of the body using X-rays and a computer. CT scans are also referred to a computerized axial tomography. CT produces data that can be manipulated in order to demonstrate various bodily structures based on their ability to absorb the X-ray beam.

The first CT scan was installed in 1974. CT scan have vastly improved patient comfort because a scan can be done quickly. Improvements have led to higher-resolution images, which assist the doctor in making a diagnosis. Modern scanners allow this volume of data to be reformatted in various planes or even as volumetric (3D) representations of structures (6).

Figure 2.7 Computed tomography (CT) scan

2.1.2.1 Computed tomography simulator (CT-sim)

Simulation is a planning session done before the external beam radiation treatment is given. A machine called a simulator is used to set up the treatment plan and the treatment area. Simulators have many modalities such as conventional Simulator, CT Simulator, MRI Simulator and PET/CT Simulator. CT simulator is the most commonly used as the gold standard simulator due to the advantages in inhomogeneity correction in treatment planning.

The CT simulator looks like a conventional CT, however, it has some special designs for radiotherapy fields, those are;

1) large aperture bore for immobilization insertion (A in fig.2.8),
2) flat couch top as the same design with treatment couch (B in fig.2.8),
3) external laser for patient positioning (C in fig.2.8),
4) virtual simulation software for treatment fields simulation and digital reconstructed radiograph (DRR) images generating for treatment field verification purpose (fig.2.9).

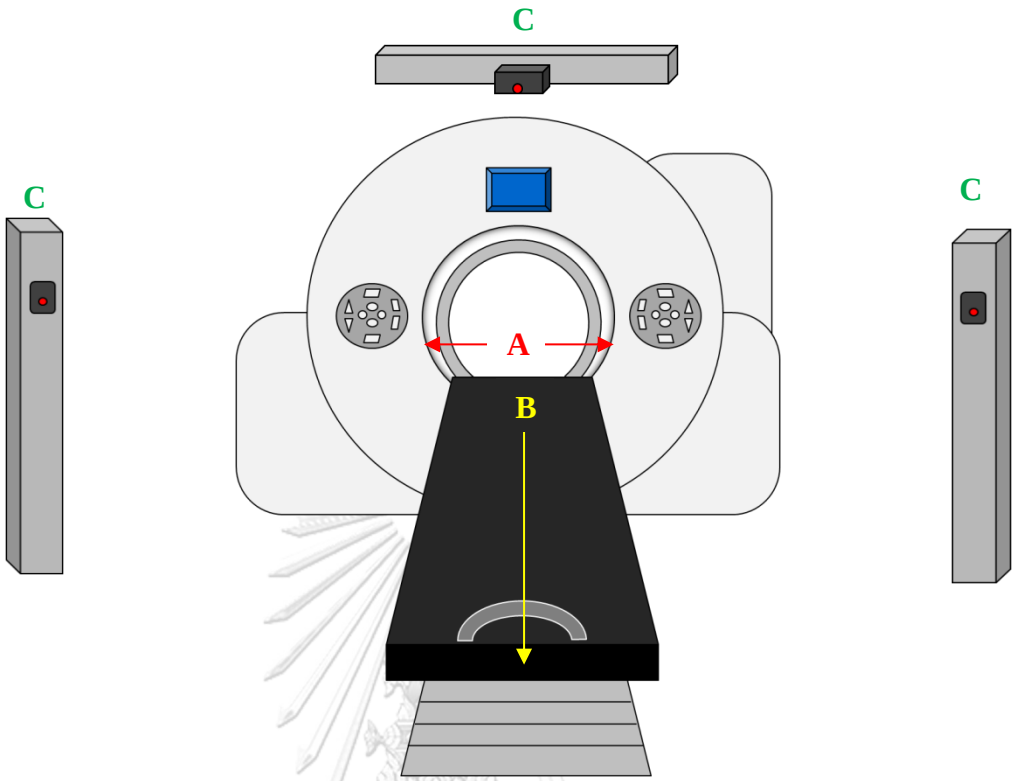

Figure 2.8 CT simulator scan;
A) large aperture bore, **B)** flat couch top and **C)** external laser system

Figure 2. 9 Example of virtual simulation software and digital reconstructed radiograph image.

2.1.2.2 Dual energy computed tomography (DECT) simulator

Dual energy CT (DECT) scans are nowadays available used a simulation machine in radiotherapy field. It involves the acquisition of CT data sets from two different x-ray spectra. For the clinical it related applications for improved dose calculation accuracy of brachytherapy and proton therapy, metal artifact reduction techniques and normal tissue characterization (3).

Dual energy CT utilises two separate energy sets to examine the different attenuation properties of matter, having a significant advantage over traditional single energy CT. Independent attenuation values at two energy sets can create virtual non-contrast images from contrast enhanced imaging as well as delineate the composition of disease (7).

There are many different dual energy technologies available (fig.2.10):

- Dual tubes with or without beam filtration
- Rapid voltage switching with single tube
- Dual-layer detector with single tube
- Single tube with split filter
- Single tube with sequential dual scans

Dual tubes with or without beam filtration (8)

This method requires a dual-source CT system in which each X-ray tube produces different X-ray energy spectra. The most striking advantage of this method is that the tube voltage, tube current, and filter are adjustable to maximize dual-energy spectral contrast and radiation dose efficiency based on the patients' body size and diagnostic purpose.

Rapid voltage switching with single tube (8)

In this method, tube voltage is rapidly changed between 80 and 140 kVp, and the two projection data sets are collected separately for subsequent use in a projection based dual-energy reconstruction algorithm.

Dual-layer detector with single tube (8)

In this method, the unique dual-layer energy-resolving detector is used for dual-energy data acquisition. Polychromatic X-ray photons are generated by one tube; thus, dual-energy scan is performed at a single fixed-tube voltage, generally 120 kVp, unlike other methods using two different tube voltages. The inner thin layer consisting of yttrium-based scintillator absorbs low-energy photons selectively, while the outer thick layer consisting of $Gd_2O_2S_2$ absorbs high-energy photons.

Single tube with split filter (8)

In this method, a split filter is applied to a single X-ray tube at 120 kVp to obtain two separated but overlapped X-ray energy spectra (the so-called twin beam), limiting of dual-energy spectral contrast to lower levels than that achieved by a combination of 80 and 140 kVp. The split filter consists of 0.05-mm thick gold filter to decrease X-ray photon energy and 0.6-mm thick tin filter to increase X-ray photon energy.

Single tube with sequential dual scans (8)

In this method, dual-energy CT data with spiral or sequential scanning are acquired simply twice sequentially with two different tube voltages, usually 80 and 140 kVp. Sophisticated CT hardware is not required. However, the method is greatly limited by the greatest temporal difference between the two X-ray energy spectra precluding many dual-energy evaluations involved in contrast enhancement and moving body parts.

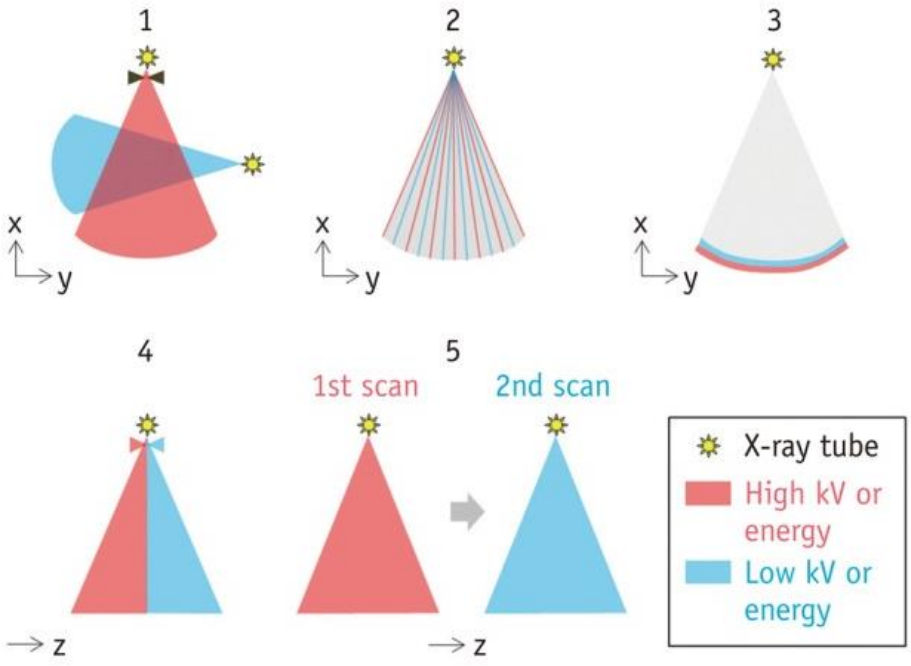

Figure 2.10 Illustration of five different methods of dual-energy CT data acquisition.
(1 = dual tubes with or without beam filtration, 2 = rapid voltage switching with single tube, 3 = dual-layer detector with single tube, 4 = single tube with split filter, 5 = single tube with sequential dual scans)

2.1.3 Computed tomography image (CT image)

CT image has been used to a gold standard for radiotherapy treatment planning because it provides the good information of bone definition, accurate geometry and supply the CT number (HU) information.

The value of a pixel in CT is a CT number measured in term of Hounsfield units (HU). The CT number is directly related to the linear attenuation coefficient μ. Water is defined to be 0 HU, and air is defined to be -1000 HU (9).

CT number depends on the quality of the X-ray beam, the attenuation property of a medium, beam energy, density, atomic number (10) and the values can differ between scanners. Even for a single scanner, CT numbers for the same tissue depend on the kV setting and beam filtration.

The precise calculation of dose distribution in radiotherapy can be performed on the basis of knowledge of the electron density of the tissues. The heterogeneity of the patient's body is one of factors influence on the dose distribution. X-ray CT provides information on the attenuation of radiation by the patient's tissues in a form of CT number (HU) that related to electron density (ρ_e). The ρ_e is very important for tissue inhomogeneity correction in treatment planning system for megavoltage beam range due to Compton interaction. CT number values usually convert to relative electron density values and displayed with calibration curve (HU- ρ_e relationship curve) as shown in fig.2.11.

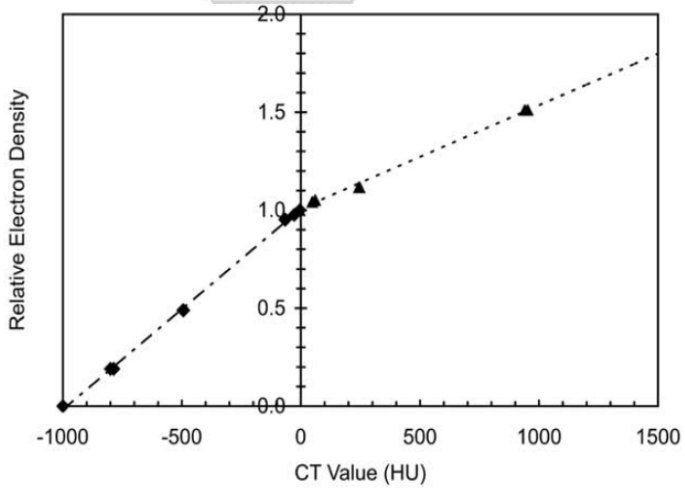

Figure 2.11 HU- ρ_e calibration curve

2.1.4 Inhomogeneity correction (11)

Inhomogeneity impacts on the attenuation of primary radiation and the distribution of radiation scatter. For megavoltage energies, attenuation of the Compton Effect depends on electron density and most difficulties arise in areas of reduced density such as air cavities or the lung. Kilovoltage beams encounter problems with high Z materials due to increase attenuation through the photoelectric effect.

2.1.4.1 Air cavity

There are many air cavities within the body, for example, the oral cavity, the pharynx, the nasal cavity, and the paranasal sinuses. Air cavities cause difficulty as there is minimal attenuation of primary radiation, and therefore decreased dose generation. This causes electronic disequilibrium and loss of dose in regions close to the inhomogeneity.

2.1.4.2 Lung

Lung consists of air and soft tissue. Lung tissue has an equivalent atomic number to soft tissue, while alveolar air spaces has lesser dense than soft tissues. The reduced density of lung leads to decrease attenuation of the primary radiation beam, which in turn leads to decrease production of radiation scatter. There is therefore a loss of electronic equilibrium within the lung unless the field is sufficiently large to create sufficient scattered radiation. The penumbra is also enlarged due to decrease attenuation of radiation scatter.

2.1.4.3 Bone

Bone has a higher atomic number than soft tissues and the electron density is also higher. Bone mineral causes increased attenuation. For kilovoltage beams the attenuation is due to increase density and the photoelectric effect, leading to increase production of radiation scatter that increases dose to bone mineral by 2 to 4 times. For megavoltage beams the attenuation only occurs to the increased density of bone.

Soft tissue within bone (bone marrow) also receives much higher dose than would be expected from kilovoltage x-rays. Unlike the bone mineral, it also receives slightly higher doses than expected from megavoltage beams due to the increased electron density per gram.

At the junction of bone and soft tissue, there is an increase in dose due to backscatter of electrons from the bone surface. This leads to a higher dose for a few millimeters on the transmission side of the bone.

- On the lung side
    - The increased density of bone relative to lung, there will be significantly more electrons generated per centimeter in bone than lung.
    - At the interface, these electrons may escape the bone tissue and enter the lung
    - This leads to an increased number of electrons relative to the lung tissue and a loss of electronic equilibrium
    - This leads to an increased dose on the lung side of the interface

- On the bone side
    - The decreased density of lung relative to bone, there will significantly fewer electrons generated per centimeter in lung than bone
    - There will be a loss of electronic equilibrium on the bone side of the interface due to decreased scatter from the lung
    - This will cause a decreased dose on the bone side of the interface

2.1.4.4 Prosthesis

Most prostheses are made from a metallic number with a relatively high atomic number. This can lead to increase dose at the junction of the prosthesis and soft tissue as well as causing increased attenuation due to the photoelectric effect or increased density. The artifact on CT imaging produced by metallic prostheses may make delineation of treatment volumes as well as calculation of dose distributions unreliable.

The tissue-air ratio method (TAR) and isodose shift method described for correcting dose in the presence of surface contour irregularity can also be used for inhomogeneity corrections. The TAR method alters dose by converting the inhomogeneity to a water equivalent material, therefore making the point beyond the inhomogeneity effectively closer or further away from the surface.

The equivalent tissue-air ratio method is the most complex and considers the effects of the inhomogeneity on both scattered and primary radiation. Modern treatment planning systems use dose kernels to adjust for inhomogeneities. Monte Carlo simulation (modeling of individual photons and their interactions) offers the best attempt at predicting dose distribution but is limited by computing power.

2.1.5 Treatment techniques

2.1.5.1 Three dimensional-conformal radiation therapy (3D-CRT)

3D-conformal radiation therapy is a cancer treatment that shapes the radiation beams to match the shape of the tumor. In the past, radiation beams only matched the height and width of the tumor for expose radiation. Advances in imaging technology have made it possible to locate and treat the tumor more precisely. Conformal radiation therapy uses the targeting information to focus precisely on the tumor, while avoiding the healthy surrounding tissues. This exact targeting makes it possible to use higher levels of radiation in treatment. More radiation is more effective in shrinking and killing tumors (12). The dose distribution of 3D-CRT with 4-field box technique of prostate case is shown in fig.2.12.

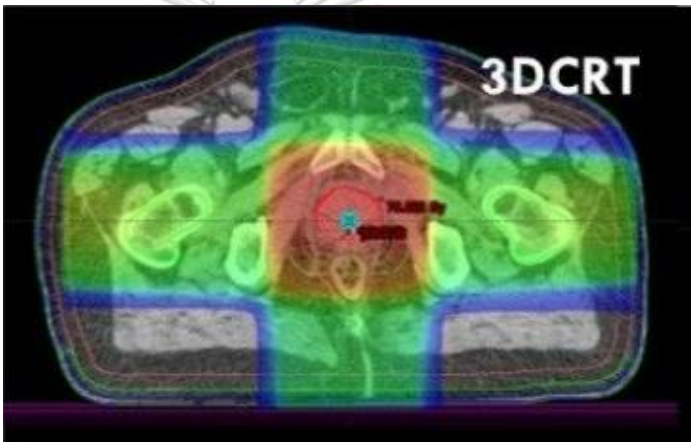

Figure 2.12 The dose distribution of 3D-CRT technique in prostate case.

2.1.5.2 Intensity modulated radiation therapy (IMRT)

Intensity modulated radiation therapy (IMRT) is a type of advanced conformal radiotherapy. Conformal radiotherapy shapes the radiation beams to closely fit the area of the cancer. IMRT can form shapes that fit precisely around the treatment area. The multileaf collimator (MLC) can move to modulate the beam intensity in each gantry angle. This means that the tumor receives a very high dose and normal healthy cells nearby receive a much lower dose compare with 3D-CRT. Each radiotherapy beam is divided into many small beamlets that can vary their intensity. This allows different doses of radiation to be given across the tumor. IMRT can also create a U shaped (concave) area at the edge of the radiotherapy field. This avoids high radiation doses to structures that would otherwise be damaged by the radiotherapy. So IMRT can reduce the risk of long term side effects (13). It is very helpful in areas such as the head and neck, for example to avoid the spinal cord or salivary glands. The dose distribution of IMRT of prostate plan is shown in fig.2.13.

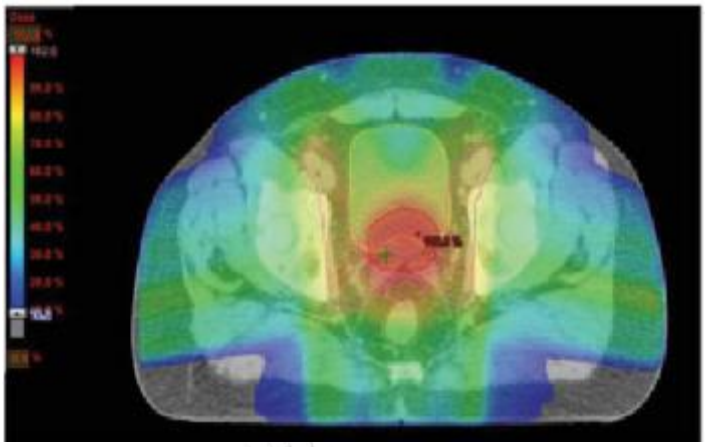

Figure 2.13 The dose distribution of IMRT technique in prostate cancer.

2.1.5.3 Volumetric modulated arc therapy (VMAT)

Volumetric modulated arc therapy (VMAT) is a novel radiation technique. The radiotherapy machine rotates around the patient during treatment. The machine continuously reshapes and changes the intensity of the radiation beam as it moves around the body. VMAT can achieve highly conformal dose distributions with improved target volume coverage and sparing of normal tissues compared with conventional radiotherapy techniques using MLC movements, dose rate and gantry speed variation. VMAT also has the potential to offer additional advantages, such as reduced treatment delivery time compared with conventional static field intensity modulated radiotherapy (IMRT) (14). The clinical worldwide use of VMAT is increasing significantly. The dose distribution of VMAT plan prostate cancer patient is shown in fig.2.14.

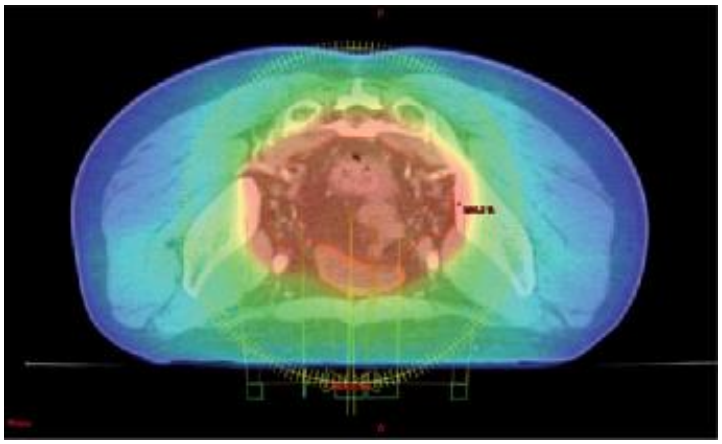

Figure 2.14 The dose distribution of VMAT technique in prostate cancer.

2.1.6 Plan evaluation

2.1.6.1 Gamma index (γ) evaluation

The gamma method, as presented by Low et al. (15), was designed for the comparison of two dose distributions: one is defined to be the reference information ($D_r(\boldsymbol{r})$) and the other is queried for evaluation ($D_r(\boldsymbol{r})$). Figure 2.15 shows a schematic representation of the gamma analysis tool for two dimensional dose distribution evaluations. The acceptance criteria are denoted by ΔD_M for the dose difference and Δd_M for the distance to agreement. For a reference point at position $\mathbf{r}_r$, receiving dose D_r, the surface representing these acceptance criteria is an ellipsoid defined by:

$$1 = \sqrt{\frac{\Delta r^2}{\Delta d_M^2} + \frac{\Delta D^2}{\Delta D_M^2}}$$

where $\Delta r = |\mathbf{r}_r - \mathbf{r}_c|$ is the distance difference between the reference and compared point

and $\Delta D = D_c(\mathbf{r_c}) - D_r(\mathbf{r}_r)$ is the dose difference at the position $\mathbf{r_c}$ relative to the reference dose D_r in $\mathbf{r}_r$. For the compared distribution to match the reference dose in $\mathbf{r}_r$, it needs to contain at least one point ($\mathbf{r_c}$, D_c) lying within the ellipsoid of acceptance, i.e. one point for which:

$$\Gamma_r(\boldsymbol{r_c}, D_c) \equiv \sqrt{\frac{\Delta r^2}{\Delta d_M^2} + \frac{\Delta D^2}{\Delta D_M^2}} \leq 1$$

A quantitative measure of the accuracy of the correspondence is determined by the point with the smallest deviation from the reference point, i.e. the point for which $\Gamma_r(\boldsymbol{r_c}, D_c)$ is minimal. This minimal value is referred to as the quality index $\gamma(\mathbf{r}_r)$ of the reference point.

The pass–fail criterion therefore becomes

$\gamma(\mathbf{r}_r) \leq 1$, correspondence is within the specified acceptance criteria,

$\gamma(\mathbf{r}_r) > 1$, correspondence is not within specified acceptance criteria.

An implicit assumption is made that once the passing criteria are selected, the dose difference and DTA analyses have equivalent significance when determining calculation quality.

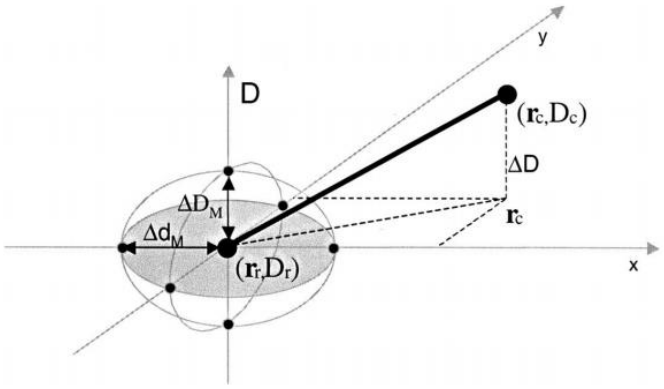

Figure 2.15 Schematic representation of the theoretical concept of the gamma evaluation method. The reference and compared dose distributions are denoted by ($\mathbf{r}_r$, D_r) and ($\mathbf{r}_c$, D_c), respectively. The criteria defining the ellipsoid of acceptance are denoted by the dose difference tolerance ΔD_M and the maximal distance to agreement Δd_M.

2.2 Review of related literatures

In 2010, Witold S. et al., (2) studied about the dependence of CT numbers on relative electron density of tissue-equivalent materials (HU-ρ_e relationship) that was measured for several general-purpose CT systems (single-slice, multislice, wide-bore multislice), for radiotherapy simulators with a single-slice CT and kV CBCT (cone-beam CT) options, as well as for linear accelerators with kV and MV CBCT systems. Electron density phantoms of four sizes were used. Measurement data were compared with the standard HU-ρ_e relationship predefined in two commercial TPSs, namely Oncentra MasterPlan and Varian Cadplan.

The results showed that HU-ρ_e relationships obtained with all of the general-purpose CT scanners operating at voltages close to 120 kV were very similar to each other and close to those predefined in TPS. There was some dependency of HU values on tube voltage, especially for bone-equivalent materials. For a given tube voltage, differences in results obtained for different phantoms were larger than those obtained for different CT scanners. For radiotherapy simulators and kV CBCT systems, the information on ρ_e was much less precise because of the poor uniformity of images. For MV CBCT, the results were significantly different than that from kV systems due to the different in energy spectrum of the beam.

In 2015, Rhee D. et al., (4) studied in the effects of the difference in tube voltage of the CT scanner on dose calculation. In radiation therapy, CT number, which is directly proportional to the linear attenuation coefficient, is required to be converted to electron density for radiation dose calculation for cancer treatment. However, if various tube voltages were applied to take the patient CT image without applying the specific CT number to electron density conversion curve, the accuracy of dose calculation would be unassured. In this study, the changes in CT numbers for different materials due to change in tube voltage were demonstrated and the dose calculation errors in percentage depth dose (PDD) and a clinical case were analyzed. The maximum dose difference in PDD from TPS dose calculation and Monte Carlo simulation when applying the same CT number to electron density conversion curve to 80 kVp and 140 kVp images were 1.3 % and 1.1 %, respectively. In clinical case, the different CT number to electron density conversion curves from 80 kVp and 140 kVp were applied to the same image. The maximum differences at the central region of the phantom in mean, maximum and minimum doses were 1.1 %, 1.2 and 1.0 %, respectively and at the peripheral region of the phantom were 0.6 %, 0.9 % and 0.8 %, respectively.

In 2016, Indra J. et al., (16) studied an overview of inhomogeneity correction in the context of CT scanning and a new evaluation tool, difference volume dose-volume histogram (DVH), dV-DVH. They concluded that the variation of CT number versus scanning parameters and CT scanner vendors is different. CT numbers for the same material from different CT scanners are expected to be variable. However, for low-density media, CT number changes are minimal with scanners and X-ray energies but deviations could be significant for high-density materials. A higher tube voltage gives lower CT number, while other parameters such as reconstruction FOV and scanner aperture have little effect on CT number. For low-density tissues, inhomogeneity correction can be successfully (±2%) applied with a single CT – electron density table for 120–140 kVp. Larger variation in dose coverage was observed for high-density tissues between different tube voltages.

For lungs, changes in CT number are minimal among scanners and CT parameters. Dosimetric differences for lung and prostate cases are usually insignificant (< 2%) in three-dimensional conformal radiation therapy (3D-CRT) and < 5% for intensity-modulated radiation therapy (IMRT) with CT parameters. Thus, should be performing more strict calibrations corresponding to tube energy especially when IMRT is used.

The dV-DVH is a simple and useful tool for dosimetric comparison as it enhances graphically the small differences between the DVHs that are superimposed on each other. Validity of acquiring different CT data for planning should be evaluated based on necessity and actual gain in dosimetry.

CHAPTER III

RESEARCH METHODOLOGY

3.1 Research design

This study is an observational analytical study research.

3.2 Research design model

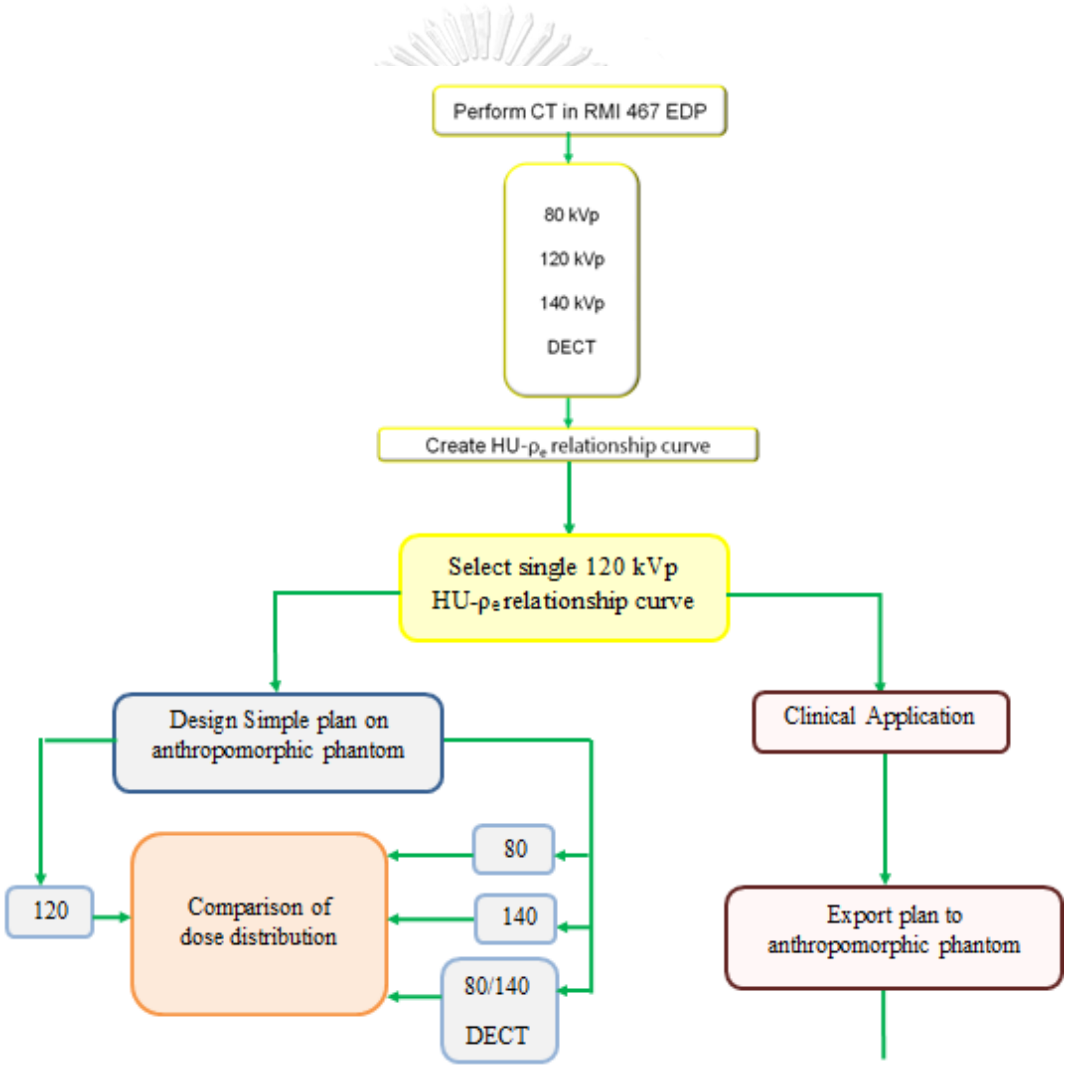

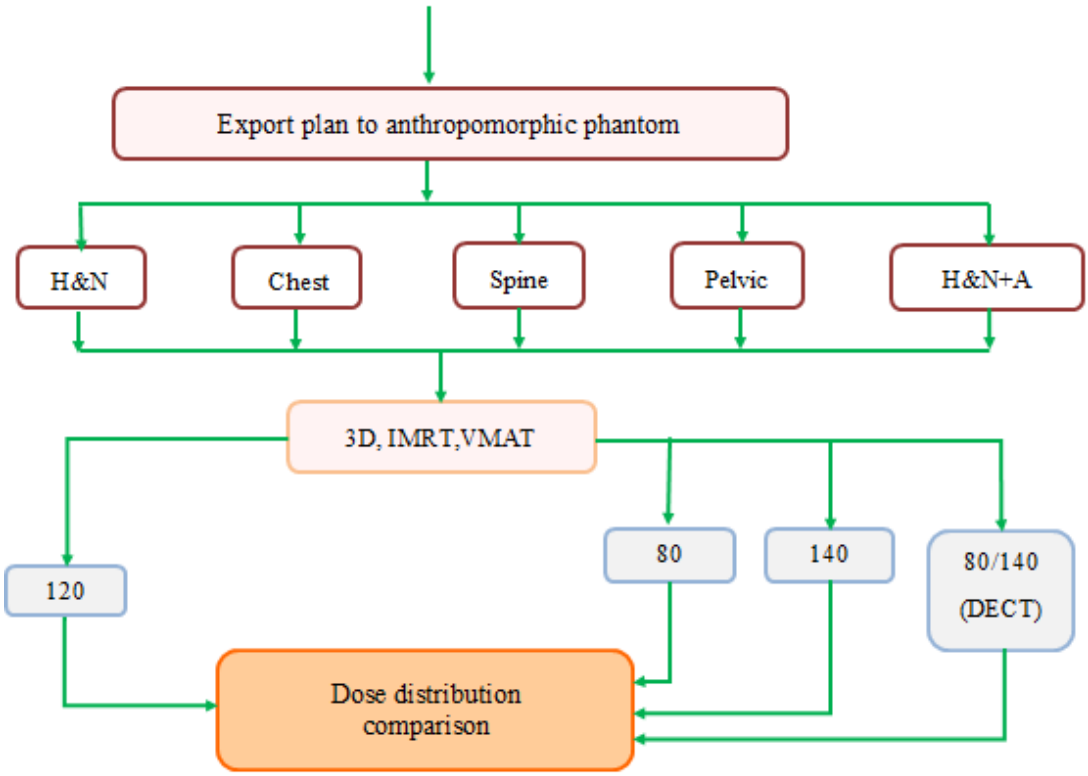
Export plan to anthropomorphic phantom
H&N
Chest
Spine
Pelvic
H&N+A
3D, IMRT,VMAT
120
80
140
80/140
(DECT)
Dose distribution
comparison

3.3 Conceptual framework

The dose distribution is affected by several factors such as HU-ρ_e relationship curve, complicate of plan, treatment regions, and treatment techniques. The diagram of conceptual framework is shown in fig.3.1.

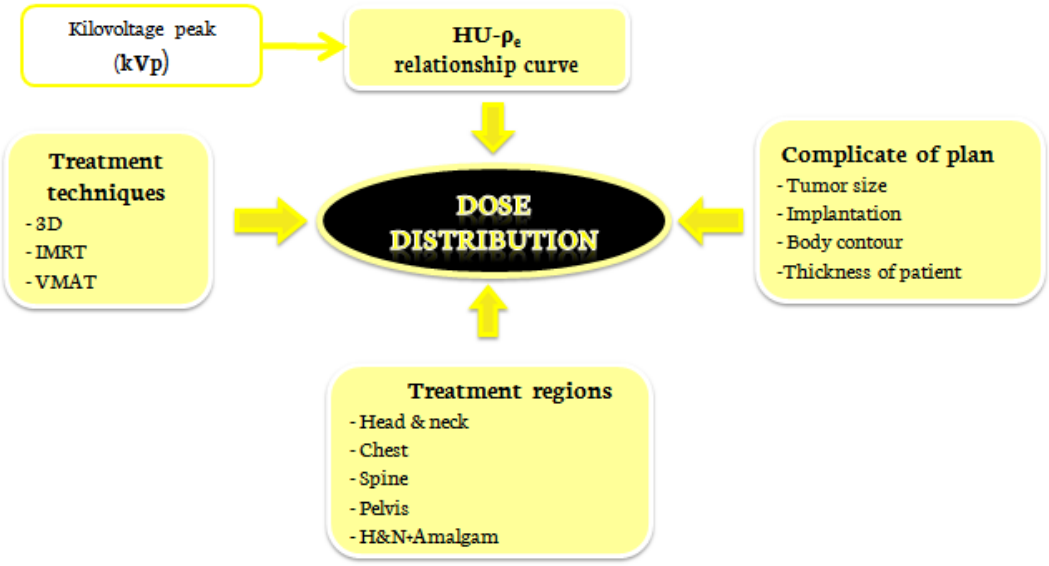

3.4 Keywords

- CT simulator
- DECT
- CT number and electron density
- Gamma index

3.5 Research questions

What are the dosimetric effects on different kVp setting for CT images using single HU-ρ_e relationship curve in head and neck, chest, spine and pelvic regions?

3.6 Materials

The materials used in this study were supplied from the Division of Radiation Oncology, King Chulalongkorn Memorial Hospital.

3.6.1 CT simulator

The DECT simulator (SOMATOM Definition AS 64-slice configuration, Siemens Healthcare GmbH, Erlangen, Germany) as shown in fig.3.2, was used in this study. Aperture bore diameter size of 800 mm is designed for immobilization insertion. The distance from tube to isocenter is 595 mm. The distance from tube to detector is 1085 mm. Tube voltage setting is 80, 120, 140 kVp and 80/140 kVp combination for DECT option. The range of mA setting is 20-666 mA. The reconstruction matrix size is 512x512.

Figure 3.2 Dual-energy CT (Siemens-SOMATOM Definition AS (64-slice configuration))

3.6.2 Electron density phantom (17)

The Gammex 467 Tissue Characterization Phantom (JRT Associates, NY, USA) as shown in fig.3.3, can be used to provide an accurate correction for tissue inhomogeneities. This phantom can be used to establish the relationship between the electron density of various tissues and their corresponding CT number.

This phantom consists of a solid water disk with the size approximately equal to average pelvis. A matrix of 16 holes (13 different tissues characteristica) in the disk hold interchangeable rods is made of various tissue and water simulating materials. The physical density (gr/cm^3) and electron density relative to water of the rod materials are provided on a specification sheet with each phantom.

Scanning the electron density phantom on a periodic basis provides a useful data for QA program of both the CT scanner and treatment planning system.

Figure 3.3 Electron density phantom (Gammex 467)

3.6.3 Anthropomorphic phantom

Anthropomorphic RANDO® phantom (The Phantom laboratory, Salem, NY, USA) as exhibited in fig.3.4, is molded of tissue-equivalent material**.** RANDO® phantom incorporates the materials to simulate various tissues such as muscle, bone, lung, and air cavity. RANDO® phantom provides the detailed mapping of dose distribution that is essential for evaluating radiotherapy treatment plans. There are two RANDO® models: RANDO® Man and RANDO® Woman. RANDO® phantoms are constructed with a natural human skeleton cast inside material that is radiologically equivalent to soft tissue (18).

RANDO® phantom is transected-horizontally into 2.5 cm thick slices. Each slice has holes which are plugged with bone equivalent, soft tissue equivalent or lung tissue equivalent pins which can be replaced by TLD holder pins. The holder pins are ordered separately (19).

Figure 3.4 Anthropomorphic RANDO® phantom

3.6.4 Treatment planning system (TPS) (20)

The Eclipse™ treatment planning system version 11.0.31 (Varian Medical Systems, Inc., Palo Alto, CA, USA) as displayed in fig.3.5, is an integrated and comprehensive treatment planning system supporting radiation treatment such as photon, FFF beams, protons, electrons, low-dose-rate brachytherapy, and cobalt therapy. There are two photon dose calculation algorithms: Analytical Anisotropic Algorithm (AAA) and Acuros XB algorithm. Eclipse™ TPS allows clinicians to efficiently create and verify the best treatment plans for their patients.

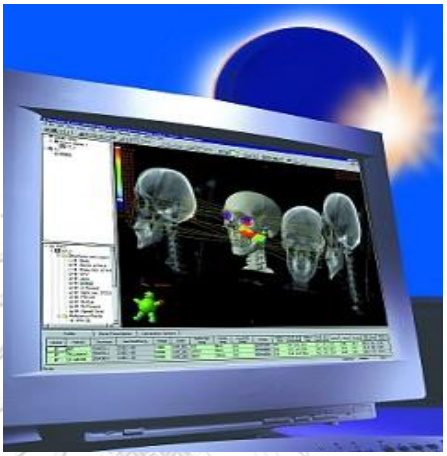

Figure 3.5 Eclipse™ treatment planning system

3.6.5 Amalgam

The amalgam, as can be seen in fig.3.6, is a mixture of two or more metals (alloy) with mercury which has been purified by distillation to remove impurities. Alloy can be a liquid, a soft paste or a solid, depending upon the proportion of mercury.

In the field of dentistry, the amalgam has been widely used due to several number of advantageous such as inexpensive, easy to use and manipulate during placement. In addition, it remains soft for a short time so enables to be packed in any irregular volume. The amalgam also forms a hard compound. The amalgam has greater longevity when compared to other direct restorative materials (21).

Figure 3.6 Example of amalgam for dentistry.

3.6.6 SNC patient software

Sophisticated treatment options such as Arc, Helical, IGRT, IMRT, and SRS demand equally to the sophisticated patient specific QA. Modern patient plans are often collections of small beamlets with very steep dose gradients. Since these dose gradients are tightly conform to patient anatomy and PTV, an accurate verification of the dose gradient is critical (22). SNC patient software (SUN Nuclear corporation, Melbourne, FL, USA) as shown in fig.3.7, is able calculate the gamma passing rate for the entire irradiated volume as well as the gamma passing rate for each corresponding ROI. This study employed SNC patient software to evaluate 2D planar dose difference (using gamma index) of all treatment plans.

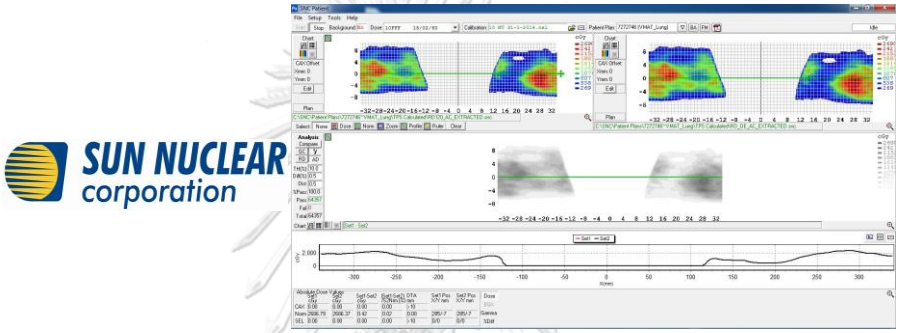

Figure 3.7 SNC patient software

3.7 Method

3.7.1 HU-ρe relationship curves

A. Gammex 467 electron density phantom (EDP) was scanned by CT scan with scanning parameters of 120 kVp, 300 mAs in axial mode of 1 cm slice thickness. External lasers were set at center of EDP as displayed in fig.3.8(a).

B. CT scan was repeated by changing to DECT option (80/140 kVp), 80 kVp and 140 kVp with the same scanning parameters of 120 kVp as shown in fig.3.8(b).

C. ROI in each material of CT image was drawn to record the CT number values as illustrated in fig.3.8(c).

D. The relationship curve between CT number of various materials in EDP and electron density value in each tube voltage setting was plotted.

E. The HU-ρ_e relationship curve of 120 kVp was used as the standard HU-ρ_e relationship curve.

F. The standard HU-ρ_e curve was applied into Eclipse^{TM} treatment planning system for photon dose calculation.

(a)

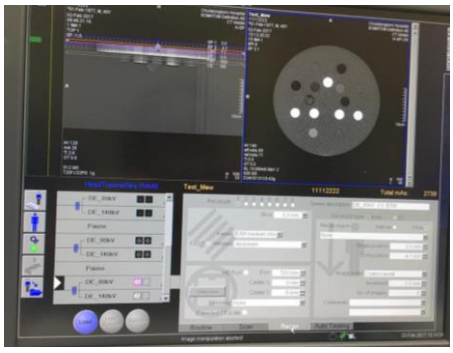

(b)

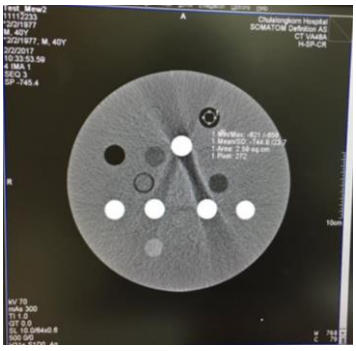

(c)

Figure 3.8 Gammex 467 EDP setup for CT-SIM scanning

3.7.2 Anthropomorphic RANDO® Phantom scanned on various kVp setting

A. The 0.5 cm. axial slice thickness of Anthropomorphic RANDO® phantom was scanned using CT scan with exposure parameter of DECT option, 80 kVp, 120 kVp, and 140 kVp with AEC mAs setup.

B. Image from 120 kVp was utilized as a reference image**.**

C. Amalgam was inserted in anthropomorphic RANDO® phantom near the teeth location in order to represent filled dental in patients. This was scanned in H&N region with various kVp setting. Fig 3.9 illustrates the placement of amalgam in our study.

D. All images data were exported into Eclipse™ treatment planning system for photon dose calculation.

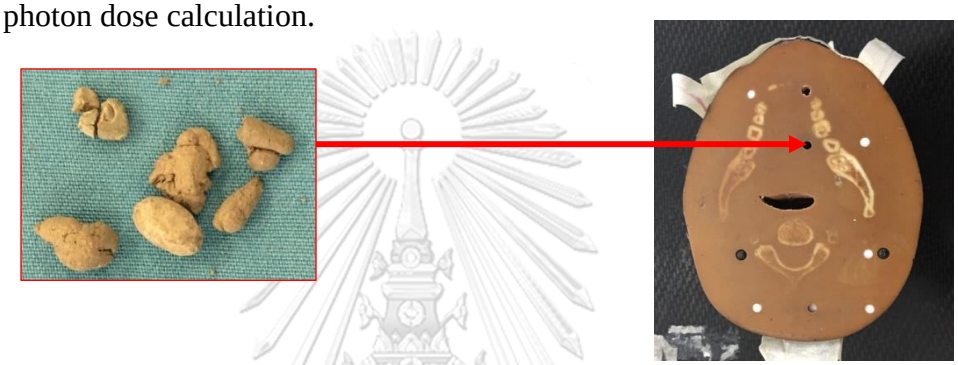

Figure 3.9 Location of amalgam insertion to anthropomorphic RANDO® phantom

3.7.3. Point dose at isocenter and dose distribution comparison

A. Five clinical plans in each 3D, IMRT and VMAT techniques in each region (H&N, chest, pelvic and H&N with amalgam regions) were exported to anthropomorphic RANDO® phantom images and were recalculated for all kVp setting images. (fig.3.10). The number of field or arc in each plan is depicted in table 3.1.

B. Point dose differences at isocenter and dose distribution difference with the reference from 120 kVp image on 120 kVp HU-ρ_e relationship curve were evaluated by using dose-volume histogram (DVH) and 2D planar dose using gamma index from SNC patient software (fig.3.11) with criteria 1%/1mm. ($\gamma_{1\%/1mm.}$).

Table 3.1 Number of field or arc in each treatment region and treatment technique *H&N+A= H&N with amalgam case

Number of field or arc in each plan				
Treatment techniques	Treatment regions			
	H&N/H&N+A*	Chest	Spine	Pelvis
3D	2 fields	2-3 fields	1-2 fields	3-4 fields
IMRT	9 fields	7-9 fields	7-9 fields	7-9 fields
VMAT	2.5-3 arcs	2.5-3 arcs	2.5-3 arcs	2.5-3 arcs

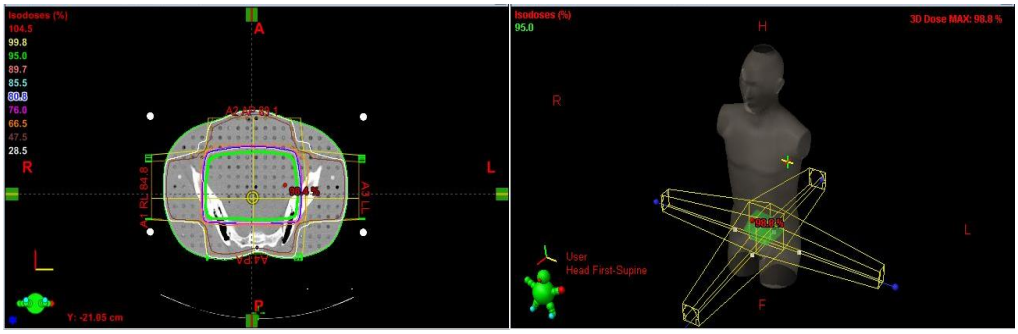

(a)

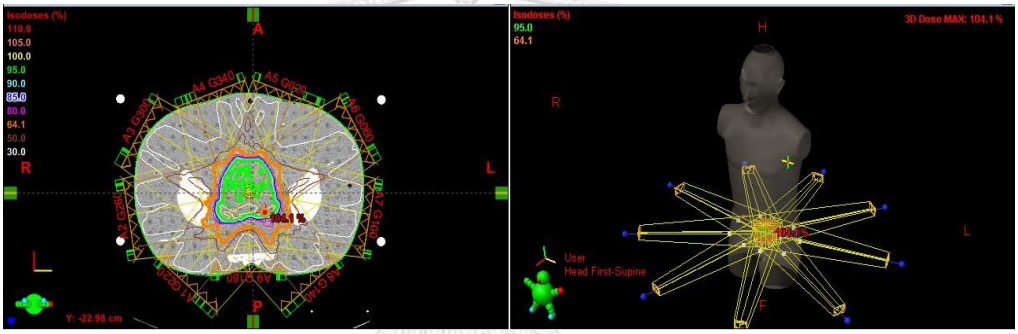

(b)

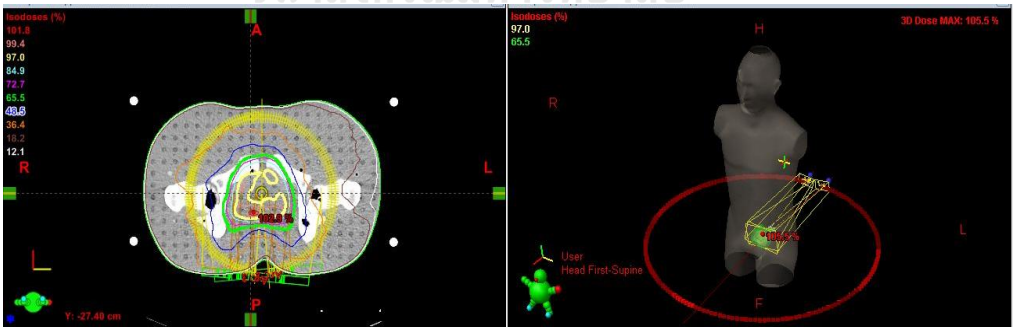

(c)

Figure 3.10 Example of clinical plan which was exported and recalculated on anthropomorphic phantom for (a) 3D technique, (b) IMRT technique and (c) VMAT technique in pelvis region.

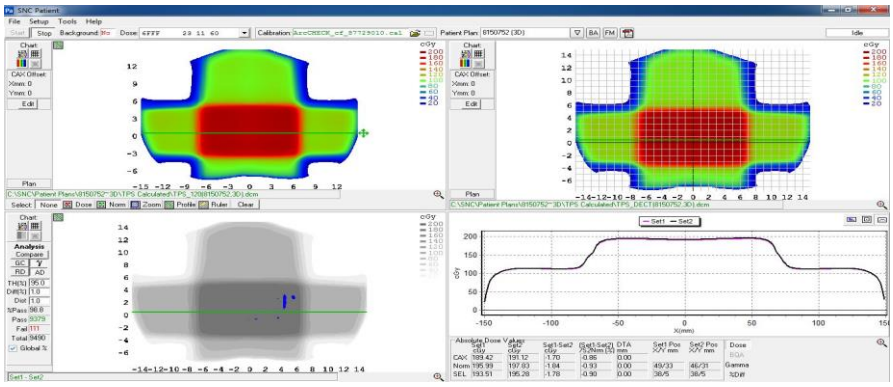

(a)

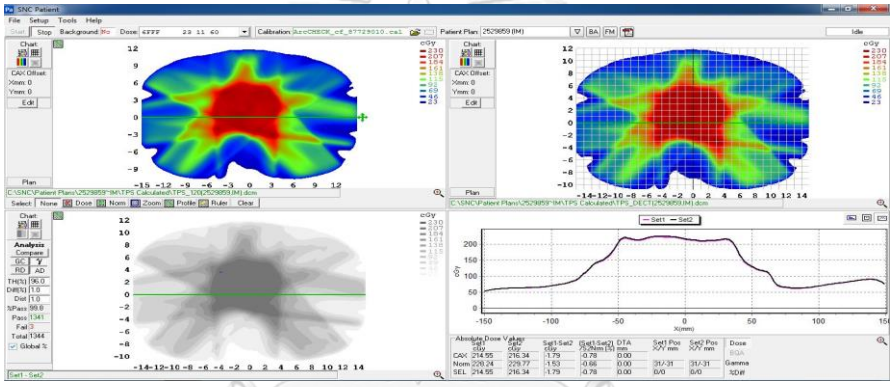

(b)

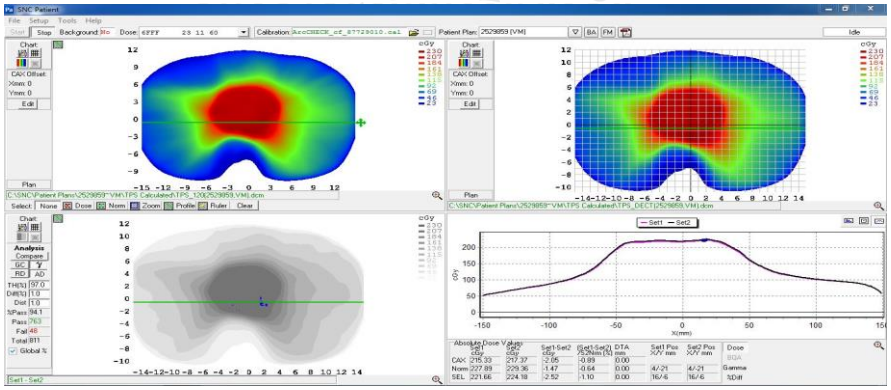

(c)

Figure 3.11 Example of 2D planar dose distribution comparison between reference image (120 kVp) and various kVp images in each treatment plan from SNC patient software for (a) 3D technique, (b) IMRT technique and (c) VMAT technique in pelvis region.

3.8 Outcome measurement

The outcomes for the determination of dose distribution were point dose difference, mean dose difference, and gamma passing rate from SNC patient**.**

There were two main variables in our study : Dependent variables and Independent variables.

- Dependent variables = Tube voltage, Treatment techniques, Treatment regions
- Independent variables = HU-ρ_e relationship curve that was scanned by 120 kVp

3.9 Data collection

All data in this thesis were undertaken using various tube voltage (DECT option, 80 kVp, 120 kVp, and 140 kVp) images of anthropomorphic RANDO® phantom in 5 treatment regions and 3 treatment techniques. Five treatment regions composed of head and neck, chest, spine, pelvic, and H&N with amalgam regions. Meanwhile, three treatment techniques were 3D, IMRT and VMAT techniques.

3.10 Data analysis

The outcomes of dose distribution in this thesis were reported as mean, percent dose difference, and standard deviation. The comparison of percent point dose difference at isocenter and gamma passing rate from each treatment plan were presented in the form of tables and bar graphs.

3.10.1 Percent point dose difference

Percent point dose difference in each treatment plan was calculated following the equation below. The tolerance should be within ±3%.

$$\%\ point\ dose\ difference = \frac{Point\ dose\ from\ various\ kVp\ plan - Point\ dose\ from\ 120\ kVp\ plan}{Point\ dose\ from\ 120\ kVp\ plan} \times 100$$

3.10.2 Gamma index

The criteria used for comparison is the evaluation of 1% dose difference and 1 mm. distance to agreement with percent prescribed dose threshold. Gamma pass tolerance should be larger than 80%.

3.11 Benefit of the study

To obtain a single CT number and electron density relationship curve which could be applied to all tube voltage CT scanning.

3.12 Ethical consideration

This research involves the dosimetric effect in 3D, IMRT and VMAT plans of radiotherapy patient. The patient data had been extracted from the image DICOM header. The research proposal has been approved by Ethics Committee of Faculty of Medicine, Chulalongkorn University (IRB No. 37060). The certificate is shown in fig.3.12.

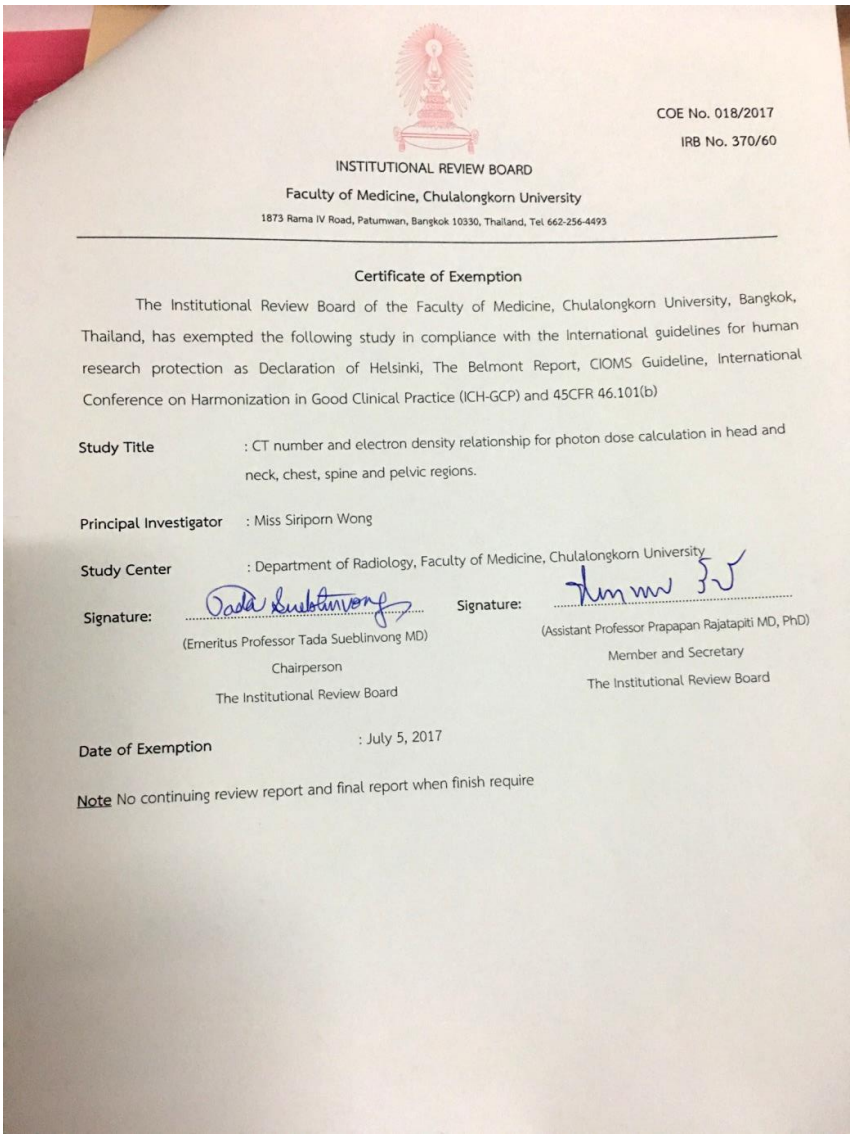

COE No. 018/2017
IRB No. 370/60

INSTITUTIONAL REVIEW BOARD
Faculty of Medicine, Chulalongkorn University
1873 Rama IV Road, Patumwan, Bangkok 10330, Thailand, Tel 662-256-4493

Certificate of Exemption

The Institutional Review Board of the Faculty of Medicine, Chulalongkorn University, Bangkok, Thailand, has exempted the following study in compliance with the International guidelines for human research protection as Declaration of Helsinki, The Belmont Report, CIOMS Guideline, International Conference on Harmonization in Good Clinical Practice (ICH-GCP) and 45CFR 46.101(b)

Study Title : CT number and electron density relationship for photon dose calculation in head and neck, chest, spine and pelvic regions.

Principal Investigator : Miss Siriporn Wong

Study Center : Department of Radiology, Faculty of Medicine, Chulalongkorn University

Signature: ..... Signature: .....

(Emeritus Professor Tada Sueblinvong MD)
Chairperson
The Institutional Review Board

(Assistant Professor Prapapan Rajatapiti MD, PhD)
Member and Secretary
The Institutional Review Board

Date of Exemption : July 5, 2017

Note No continuing review report and final report when finish require

Figure 3.12 The certificate of approval from Ethical Committee of Faculty of Medicine, Chulalongkorn University.

CHAPTER IV

RESULTS

4.1 HU-ρ_e relationship curves

The result of HU-ρ_e relationship curves with various tube voltage settings can be observed in fig.4.1. CT number values in each tissue mimicking inserts from Gammex 467 EDP are shown in table 4.1. The higher relative electron density value presented the increase CT number value and the higher tube voltage showed the lower CT number, especially in high density materials. The curves trended to linear at the relative ρ_e values less than 1 (low density materials) and presented the step near CT number in the range of 0-200, then shown the linear curve again in higher ρ_e value. The relationship curve of all kVp were superimposed in ρ_e less than 1 and the curve noticeable deviated at the relative ρ_e values more than 1 (high density materials), especially in 80 kVp and DECT curves.

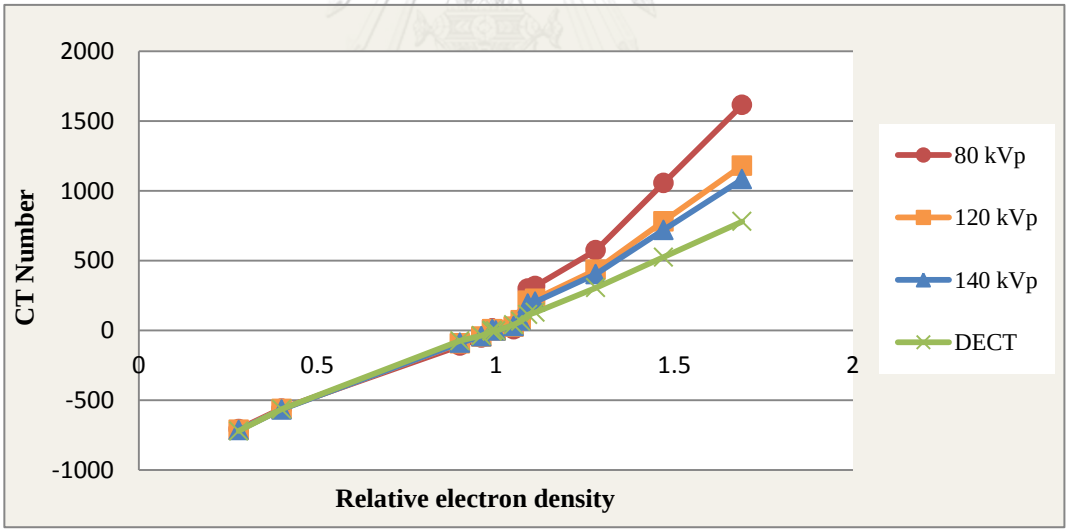

Figure 4.1 The HU-ρ_e relationship curves with various tube voltage setting.

Table 4.1 CT number values of tissue mimicking inserted from Gammex 467 EDP in each tube voltage setting

NO.	Tissue mimicking inserts	Electron density relative to water (ρ_e)	CT number (HU)			
			120 kVp (reference)	DECT	80 kVp	140 kVp
1	Lung (LN-300)	0.286	-760.7	-719.5	-744.9	-765.6
2	Lung (LN-450)	0.409	-601.1	-563.9	-592.1	-604.0
3	Adipose (AP6)	0.926	-101.4	-73.2	-133.7	-96.6
4	Breast	0.962	-47.6	-36.0	-64.2	-46.7
5	Solid water	0.991	3.6	-3.1	7.8	2.7
6	Solid water	0.991	4.1	-1.5	19.7	3.5
7	Solid water	0.991	2.4	-4.6	13.9	0.5
8	Solid water	0.991	3.6	-1.6	16.6	4.2
9	True water (H_2O)	1.000	-2.2	-3.6	-0.9	1.6
10	Brain	1.048	26.4	41.2	-0.6	30.5
11	Liver (LV1)	1.058	71.8	65.7	77.6	74.0
12	Inner bone	1.098	222.2	114.0	366.9	203.2
13	Bone (B200)	1.111	236.9	129.2	386.0	218.1
14	Bone (CB2-30% Mineral)	1.280	463.5	305.9	701.4	431.8
15	Bone (CB2-50% Mineral)	1.470	833.2	525.2	1299.5	771.0
16	Cortical Bone	1.695	1261.0	781.3	1954.7	1162.3

4.2 Point dose differences at isocenter

The raw data of point dose and point dose differences at isocenter of all plans are shown in table A.1 (appendix) and table 4.2, respectively. The maximum point dose difference at isocenter was 1.3% from DECT image of pelvic case with IMRT technique, while the minimum was 0.0%, which was noticeable from many cases. According to treatment regions, the average point dose differences at isocenter of DECT, 80 kVp and 140 kVp images compared to 120 kVp reference image were 0.7±0.4%, 0.4±0.3% and 0.3±0.3% for head and neck, 0.5±0.3%, 0.3±0.1% and 0.2±0.2% for chest, 0.6±0.2%, 0.5±0.2% and 0.1±0.1% for spine, 0.9±0.2%, 0.7±0.2% and 0.2±0.1% for pelvic and 0.1±0.1%, 0.4±0.3% and 0.1±0.1% for H&N with amalgam regions, respectively. The results are shown in fig.4.2.

Table 4.2 The point dose differences of all plans in each treatment region, each treatment technique and each tube voltage setting.
*H&N+A = H&N with amalgam case

NO.	Treatment regions and techniques	Point dose differences in each tube voltage (%)		
		DECT	80 kVp	140 kVp
1	Head and neck 3D	0.0	0.0	0.8
2		0.2	0.1	0.1
3		0.6	0.3	0.0
4		1.0	0.7	0.1
5		1.0	0.7	0.7
6	Head and neck IMRT	0.9	0.3	0.1
7		0.9	0.3	0.4
8		0.6	0.3	0.1
9		1.1	0.5	1.0
10		0.2	0.1	0.1
11	Head and neck VMAT	0.6	0.2	0.1
12		1.1	0.7	0.3
13		0.3	0.8	0.2
14		0.2	0.2	0.1
15		1.1	0.7	0.2
16	Chest 3D	0.5	0.3	0.0
17		0.2	0.2	0.0
18		0.7	0.4	0.3

NO.	Treatment regions and techniques	Point dose differences in each tube voltage (%)		
		DECT	80 kVp	140 kVp
19	Chest 3D	0.5	0.5	0.1
20		0.4	0.2	0.1
21	Chest IMRT	0.1	0.1	0.1
22		0.5	0.2	0.7
23		0.6	0.3	0.1
24		1.1	0.5	0.2
25		0.2	0.1	0.1
26	Chest VMAT	0.1	0.0	0.0
27		0.5	0.4	0.1
28		0.5	0.5	0.1
29		0.2	0.2	0.1
30		1.0	0.1	0.8
31	Spine 3D	0.6	0.4	0.2
32		0.5	0.4	0.1
33		0.5	0.3	0.1
34		0.8	0.4	0.3
35		0.8	0.4	0.1
36	Spine IMRT	0.5	0.2	0.2
37		0.8	0.7	0.0
38		0.6	0.5	0.1
39		0.3	1.0	0.1
40		0.6	0.6	0.0
41	Spine VMAT	0.8	0.2	0.3
42		0.1	0.3	0.2
43		1.1	0.6	0.2
44		0.5	0.4	0.1
45		0.5	0.4	0.1
46	Pelvis 3D	0.9	0.6	0.2
47		1.0	0.6	0.2
48		0.8	0.8	0.2
49		0.8	0.8	0.3
50		0.9	0.8	0.2

NO.	Treatment regions and techniques	Point dose differences in each tube voltage (%)		
		DECT	80 kVp	140 kVp
51	**Pelvis IMRT**	0.8	0.6	0.6
52		0.8	0.7	0.1
53		0.7	0.1	0.1
54		1.3	0.9	0.2
55		1.0	0.7	0.3
56	**Pelvis VMAT**	0.9	0.6	0.2
57		0.8	0.6	0.1
58		0.9	0.7	0.1
59		1.0	0.8	0.2
60		0.9	0.7	0.2
61	**H&N+A* 3D**	0.0	0.0	0.0
62		0.1	0.0	0.0
63		0.0	0.1	0.0
64		0.3	0.6	0.3
65		0.0	0.1	0.0
66	**H&N+A* IMRT**	0.1	0.4	0.1
67		0.1	0.1	0.1
68		0.2	1.1	0.1
69		0.1	0.6	0.2
70		0.1	0.3	0.1
71	**H&N+A* VMAT**	0.1	0.3	0.1
72		0.2	0.5	0.2
73		0.1	0.2	0.1
74		0.2	0.6	0.2
75		0.1	0.6	0.1

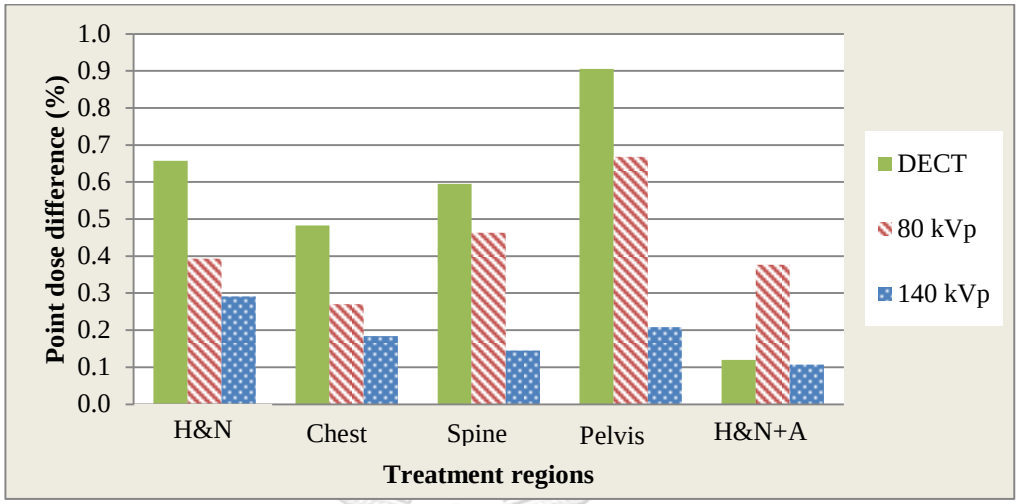

Figure 4.2 Chart of the average percent point dose difference at isocenter from all treatment techniques compared with 120 kVp image in each treatment region under various tube voltage setting.

Considering in treatment techniques, the average point dose differences of DECT, 80 kVp and 140 kVp images were 0. 5±0.4%, 0.4±0.3% and 0.2±0.2% for all cases of 3D, 0.6±0.4%, 0.5±0.3% and 0.2±0.2% for all cases of IMRT and 0.6±0.4%, 0.5±0.2% and 0.2±0.1% for all cases of VMAT, respectively. The results are shown in fig.4.3.

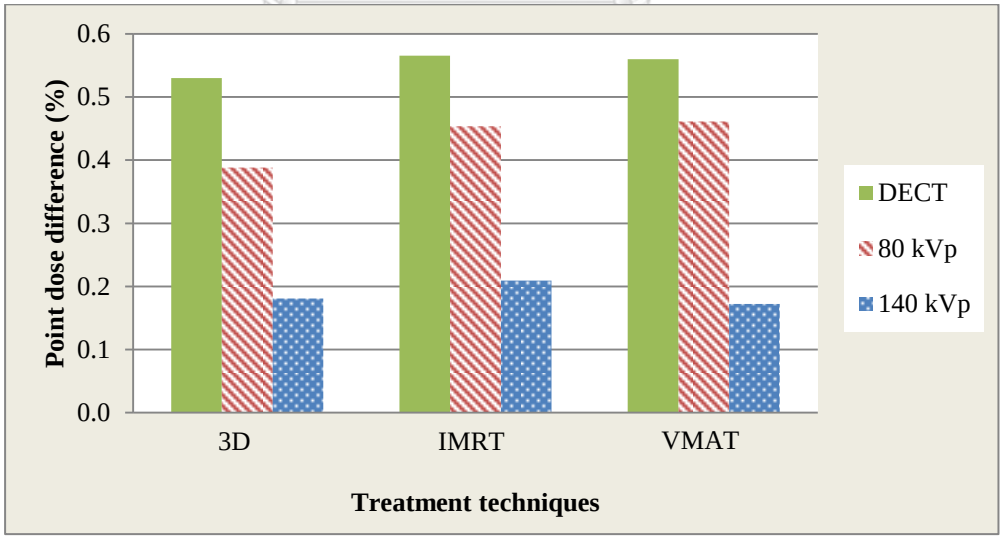

Figure 4.3 Chart of the average percent point dose difference at isocenter from all treatment regions compared with 120 kVp image in each treatment technique under various tube voltage setting.

According to tube voltage setting, the average point dose differences of DECT, 80 kVp and 140 kVp images in all regions and all techniques were 0.6±0.4%, 0.4±0.3% and 0.2±0.2%, respectively. The results are shown in fig.4.4.

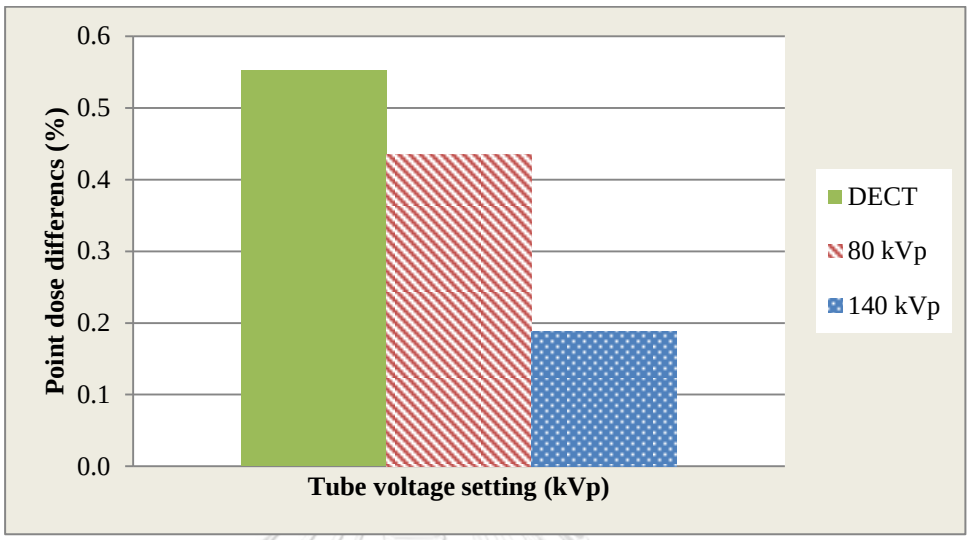

Figure 4.4 Chart of the average point dose differences from different kVp scanning images in all treatment regions and all treatment techniques.

4.3 Gamma index

The results of 2D dose differences in terms of gamma passing rate in each region and in each technique of all plans are shown in table 4.3. The maximum gamma passing rate ($\gamma_{1\%/1mm}$) was 100%, which was noticeable from many cases. The minimum gamma passing rate was 61.5% from DECT image of head and neck case with VMAT technique. Concentrating on treatment region, the average gamma passing rate (with criteria of 1%/1mm ($\gamma_{1\%/1mm.}$)) differences of DECT, 80 kVp and 140 kVp images to 120 kVp reference image were 86.1±13.4%, 99.9±0.3% and 100±0.0% for head and neck, 99.9±0.6%, 100±0.0% and 100±0.0% for chest, 99.7±0.5%, 100±0.0% and 100±0.0% for spine, 94.0±8.0%, 100±0.0% and 100±0.0% for pelvic and 100±0.0%, 99.9±0.4% and 100±0.0% for H&N with amalgam regions respectively. The results are shown in fig.4.5.

Table 4.3 The gamma passing rate ($\gamma_{1\%/1mm}$) of all plans in each treatment region, each treatment technique and each tube voltage setting compared with reference plan.

NO.	Treatment regions and techniques	Gamma passing rate (%)		
		DECT	80 kVp	140 kVp
1	Head and neck 3D	100	100	100
2		100	100	100
3		100	100	100
4		76.6	100	100
5		80.8	100	100
6	Head and neck IMRT	100	100	100
7		61.5	99.4	100
8		66.4	100	100
9		94.0	100	100
10		91.2	100	100
11	Head and neck VMAT	81.8	100	100
12		84.3	100	100
13		100	100	100
14		67.9	98.9	100
15		86.9	100	100
16	Chest 3D	100	100	100
17		100	100	100
18		100	100	100

NO.	Treatment regions and techniques	Gamma passing rate (%)		
		DECT	80 kVp	140 kVp
19	Chest 3D	100	100	100
20		100	100	100
21	Chest IMRT	100	100	100
22		100	100	100
23		100	100	100
24		100	100	100
25		100	100	100
26	Chest VMAT	100	100	100
27		100	100	100
28		97.7	100	100
29		100	100	100
30		100	100	100
31	Spine 3D	100	100	100
32		100	100	100
33		100	100	100
34		100	100	100
35		99.0	100	100
36	Spine IMRT	98.9	100	100
37		100	100	100
38		100	100	100
39		100	100	100
40		100	100	100
41	Spine VMAT	99.4	100	100
42		99.8	100	100
43		98.8	100	100
44		100	100	100
45		99.8	100	100
46	Pelvis 3D	98.8	100	100
47		80.0	100	100
48		100	100	100
49		100	100	100
50		88.7	100	100

NO.	Treatment regions and techniques	Gamma passing rate (%)		
		DECT	80 kVp	140 kVp
51	Pelvis IMRT	100	100	100
52		100	100	100
53		99.8	100	100
54		75.8	100	100
55		100	100	100
56	Pelvis VMAT	96.3	100	100
57		90.2	100	100
58		94.1	100	100
59		86.3	100	100
60		99.7	100	100
61	H&N+A* 3D	100	100	100
62		100	100	100
63		100	100	100
64		100	100	100
65		100	100	100
66	H&N+A* IMRT	100	100	100
67		100	98.3	100
68		100	100	100
69		100	100	100
70		100	100	100
71	H&N+A* VMAT	100	100	100
72		100	100	100
73		100	100	100
74		100	100	100
75		100	100	100

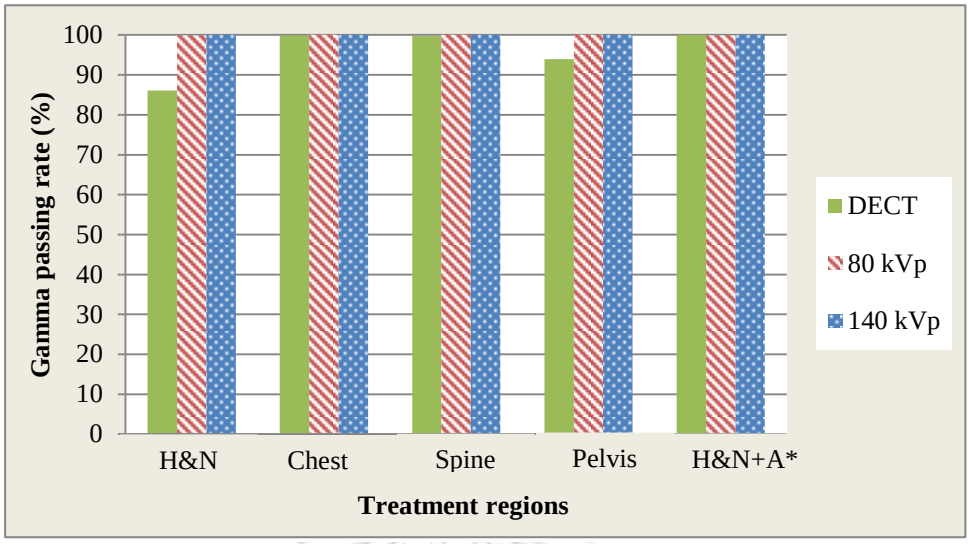

Figure 4.5 Chart of the average gamma passing rate of dose distribution in each treatment region from all treatment techniques.

Considering in treatment techniques, the average values of gamma passing rate of DECT, 80 kVp and 140 kVp images were 97.0±7.1%, 100±0.0% and 100±0.0% for all cases of 3D, 95.5±10.8%, 100±0.4% and 100±0.0% for all cases of IMRT and 95.3±8.0%, 100±0.2% and 100±0.0% for all cases of VMAT, respectively. The results are shown in fig.4.6.

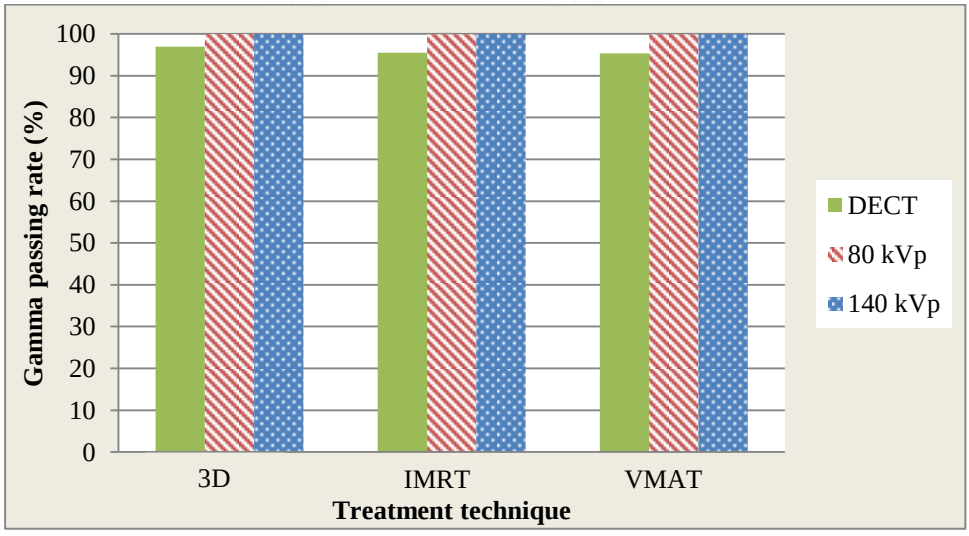

Figure 4.6 Chart of the average gamma passing rate of dose distribution in each treatment technique from all treatment regions.

The average gamma passing rate of dose distribution in all regions and all techniques of DECT, 80 kVp and 140 kVp images were 95.9 ±8.7%, 100±0.2% and 100.0±0.0%, respectively. The results are shown in fig.4.7.

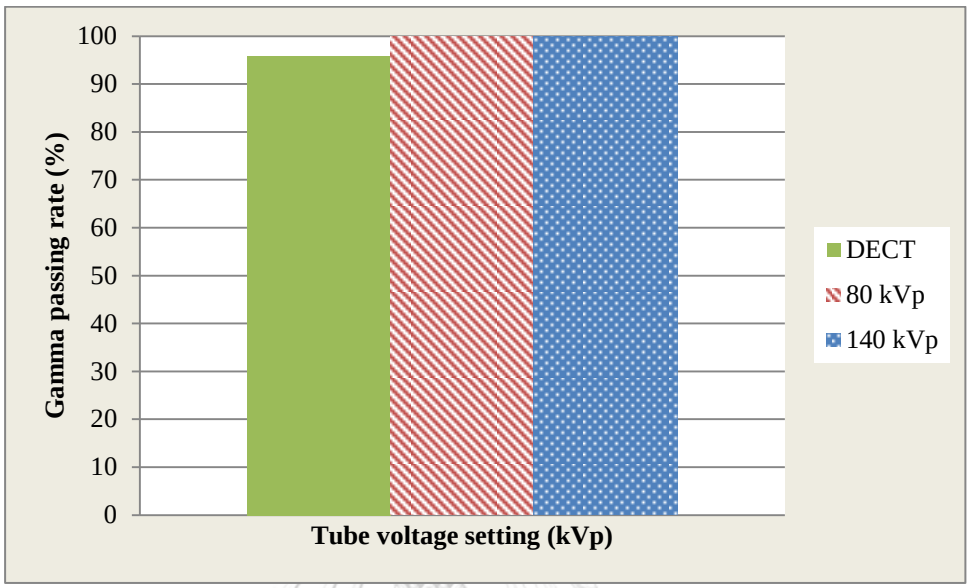

Figure 4.7 Chart of the average gamma passing rate of dose distribution from different kVp scanning images in all treatment regions and all treatment techniques.

CHAPTER V

DISCUSSION AND CONCLUSION

5.1 Discussion

5.1.1 HU-ρ_e relationship curve

From the results, the different kVp images showed the different HU values and also showed the different HU-ρ_e relationship curve due to the different X-ray attenuation from photoelectric effect in photon interaction (16, 23). The probability of photoelectric effect occurrence decreases as the atomic number decreases and incident photon energy increases, as given by the equation:

$$\frac{Z^3}{E^3}$$

where Z is the atomic number and E is the energy of the incident photon. Consequently, in the range of CT scanning energies, photoelectric interactions are less likely to occur in soft tissues, which are primarily composed from lighter elements (lower Z). A higher energy photon will decrease the probability of the photoelectric effect occurring as it will penetrate farther into the matter (24).

The different HU-ρ_e relationship curve has impacted to dose distribution, especially at high density organ (high electron density). The discrepancy became significantly for high density materials with a trend that higher kVp yielded a lower CT number due to the characteristic of HU-ρ_e relationship curves as shown in fig.4.1 (16).

5.1.2 Dosimetric effect evaluation

For this study, the dosimetric effect was evaluated by using isocenter dose differences and 2D gamma index. The results of isocenter dose differences showed the good agreement with gamma index evaluation.

5.1.2.1 Point dose difference

The DECT images presented the highest average dose differences from other energies due to the largest difference in HU-ρ_e relationship data compared with 120 kVp images (as shown in fig.4.1), however, the results in H&N with amalgam was improved in DECT image. That might be due to the reduction of artifact from high Z material from DECT image.

Pelvic region displayed the highest average dose differences than other regions because it consists of the large bone area that is the high density region. The least effect was observed in chest region because it has the lung region that consists of low electron density organ. The low electron density organ was tube voltage setting independent as shown in fig 4.1. These results agree with Indra JD. et al. (16) studied. Indra JD. et al. (16) explained the dosimetric effect that the tube voltage was the most influential factor compared to others. They investigated the impact on dose-volume coverage in real patient plans and found a very small difference for PTV coverage in lung, but relatively higher difference for the prostate case as evaluated using dV-DVH.

However, the result in H&N with amalgam was improved in DECT image compared with normal H&N case. H&N with amalgam case showed the largest average point dose difference in 80 kVp images compared with other kVp settings. It might be due to the effects of photon starvation and beam hardening of metal implants and its surrounding tissue since the introduction of CT imaging of metal artifact in low energy kVp (25).

From the treatment techniques, IMRT and VMAT in DECT image showed the highest average dose difference that might be due to the high MU and complicated leaf movements in IMRT and VMAT technique compared with others. The objective of IMRT and VMAT technique was conformal radiation dose to the tumor and spared dose to normal tissue. That causes the present in the high dose gradient.

Pelvic case with all kVp setting showed higher average point dose difference in IMRT technique compared with 3D technique. These results agree with Indra JD. et al. (16) studied, who found the differences were slightly higher in IMRT plans compared to 3DCRT. The differences based on analysis of dV-DVH in 3DCRT and IMRT for the prostate case were <2% and <5%, respectively. However, all of studied were pass criteria with the average point dose difference value less than 1% and maximum point dose difference not more than 1.3%.

5.1.2.2 Gamma index

For gamma index, the first two least average gamma passing rate ($\gamma_{1\%/1mm.}$) observed in H&N and pelvis region under DECT option setting because these 2 regions consist of many bony structures as the high density organ. Moreover, the gamma values from H&N showed the highest standard deviation values that represented the largest variation values.

The highest average gamma passing rate ($\gamma_{1\%/1mm.}$) was observed in all treatment regions (H&N, chest, spine and pelvic regions) under 140 kVp setting. The values were 100±0.0%. It might be 140 kVp images produced the closest HU-ρ_e relationship curve with 120 kVp images (as shown in fig.4.1).

When consider in treatment techniques, IMRT and VMAT techniques in DECT, 80 kVp and 140 kVp images showed the lower value compared with 3D technique due to the complication of the plans.

However, all of studied were pass criteria with the average gamma passing rate ($\gamma_{1\%/1mm.}$) value above 80% and minimum gamma passing rate not less than 61.5%.

5.2 Limitation

The limitation of this study; firstly, the radiation dose to the patients were considered, the patients cannot be scanned with different tube voltage. Secondly, the complicated level of clinical treatment plan (ex. Number of field, MUs, etc.) was not determined.

5.3 Conclusion

For head and neck, chest, spine, pelvic and H&N with amalgam regions, it is possible to apply single 120 kVp HU-ρ_e relationship curve into all tube voltage scanning images with the highest average point dose difference of 0.6±0.4% in DECT setting and average $\gamma_{1\%/1mm.}$ passing rate of 95.9±8.7%, while others kVp images show average point dose difference within 0.4±0.3% and average $\gamma_{1\%/1mm.}$ passing rate higher than 100±0.2%.

The most accurate dose calculation is necessary for treatment planning in radiotherapy field. Consequently, choosing HU-ρ_e relationship curve to apply into TPS is essential. Although the results of this study are good but still have the effect to the dosimetric especially at high density area. Therefore suitable HU-ρ_e relationship curve should be considered.

REFERENCES

1. Schneider U., Lomax A., Pedroni E. *The calibration of CT Hounsfield units for radiotherapy treatment planning.* Phys Med Biol. 1996;**41**:111-24.
2. Witold S., Zielinska D., et al. *Computed Tomography as a Source of Electron Density Information for Radiation Treatment Planning.* Strahl Onkol. 2010;**186**:327-33.
3. Wouter V., Guillaume L., Marco D., Frank V. *Dual energy CT in radiotherapy: Current applications and future outlook.* Rad and Onco. 2016;**119**:137-44.
4. Rhee DJ., Kim SW., et al. *Effects of the difference in tube voltage of the CT scanner on dose calculation.* Kor Phys Soc. 2015;**67**:123-8.
5. Sprawls P. *The Physical Principles of Medical Imaging [online] 2013* [cited 2018 2 March]. Available from: http://www.sprawls.org/ppmi2/INTERACT/.
6. Lawrence M., Davis M. *CT Scan (CAT Scan, Computerized Axial Tomography) [online]* 2006. [cited 2018 9 March]. Available from: https://www.emedicinehealth.com/ct_scan/article_em.htm.
7. Son D., Charlie C., et al. *Dual energy CT [online]* 2015. [cited 2018 15 March]. Available from: https://radiopaedia.org/articles/dual-energy-ct.
8. Hyun W., Jin M. *Dual-Energy CT: New Horizon in Medical Imaging.* Kor J Radiol. 2017;**18**(4):555-69.
9. Mark H. *CT Physics: Beam Hardening and Dual-Energy CT [online]* 2014. [cited 2018 6 March]. Available from: http://xrayphysics.com/dual_energy.html.
10. Mark H. *X-Ray Physics: X-Ray Interaction with Matter and Attenuation [online]* 2014. [cited 2018 6 March]. Available from: http://xrayphysics.com/attenuation.html.
11. Rod d. *Inhomogeneity [online]* 2010. [cited 2018 13 March]. Available from: http://ozradonc.wikidot.com/inhomogeneity-photons.
12. *3D Conformal Radiation Therapy [online]* [cited 2018 17 March]. Available from: http://hillman.upmc.com/cancer-care/radiation-oncology/treatment/external-beam/3d-conformal.
13. *Intensity-Modulated Radiation Therapy (IMRT) [online]* [cited 2018 17 March]. Available from: http://hillman.upmc.com/cancer-care/radiation-oncology/treatment/external-beam/intensity-modulated-imrt.
14. Teoh M., Clark C., Wood K., Whitaker S., Nisbet A. *Volumetric modulated arc therapy: a review of current literature and clinical use in practice.* Br J Radiol. 2011;**84**:967-96.
15. Low D., William B., Sasa M., James A. *A technique for the quantitative evaluation of dose distributions.* Med Phys. 1997;**25**:656-61.
16. Indra J., Chee W., Minsong C., Peter A. *Computed tomography imaging parameters for inhomogeneity correction in radiation treatment planning.* Med Phys. 2016;**41**:3-11.
17. *Gammex Tissue Characterization Phantom Model 467 User's Guide [online] 2004.* [cited 2018 20 March]. Available from: http://cspmedical.com/content/1021492_tissue_phantom_user_guide.pdf.
18. *The Alderson Radiation Therapy phantom [online]* 2014. [cited 2018 20 March]. Available from: http://rsdphantoms.com/rt_art.htm.
19. *RANDO Phantom* [cited 2018 20 March]. Available from: https://www.imagingsol.com.au/product/1838/RANDO-Phantom.html.
20. *Eclipse™ Treatment Planning System [online]* [cited 2018 21 March]. Available from: https://www.varian.com/oncology/products/software/treatment-planning/eclipse-treatment-planning-system.
21. *Amalgam (chemistry) [online]* [cited 2018 31 March 2018]. Available from: https://en.wikipedia.org/wiki/Amalgam_(chemistry)#Dental_amalgam.

22. *Patient QA [online]* 2013. [cited 2018 12 March]. Available from: http://work.sunnuclear.net/medPhys/patientqa/patientqa.asp.
23. Watanabe Y. *Derivation of linear attenuation coefficients from CT numbers for low-energy photons.* Phys Med Biol. 1999;**44**:2201-11.
24. Prince J., Links J. *Physical Interaction processes [online]* 2006. [cited 2018 27 March]. Available from: http://199.116.233.101/index.php/Physical_Interaction_processes#cite_note-thirtsix-4.
25. Lee Y., Park K., Song H., Kim S., Suh J. *Metal artefact reduction in gemstone spectral imaging dual-energy CT with and without metal artefact reduction software.* Eur Radiol. 2012;**22**:1331-40.

APPENDIX

Table A.1 Results of point dose at isocenter in each case.

NO.	Treatment regions and techniques	Absolute dose at isocenter in each tube voltage (%)			
		120 kVp	DECT	80 kVp	140 kVp
1	Head and neck 3D	102.8	102.8	102.8	102.0
2		315.4	316.0	315.0	315.6
3		219.8	218.4	219.2	219.7
4		533.1	538.5	529.5	533.8
5		208.0	210.1	206.5	209.4
6	Head and neck IMRT	148.3	149.6	147.9	148.4
7		102.6	103.5	102.3	103.0
8		209.2	210.4	208.6	209.4
9		145.7	147.3	145.0	147.2
10		207.1	207.6	206.8	206.8
11	Head and neck VMAT	201.1	202.3	200.6	201.4
12		198.1	200.3	196.8	198.7
13		131.8	131.4	130.8	132.0
14		206.2	206.7	205.7	206.4
15		210.0	212.3	208.5	210.5
16	Chest 3D	275.4	276.9	274.6	275.5
17		359.0	359.6	358.4	359.1
18		319.6	321.7	318.4	320.4
19		292.6	294.2	291.0	292.9
20		319.8	321.1	319.2	320.1
21	Chest IMRT	313.0	313.3	312.7	313.3
22		244.2	245.3	243.7	245.8
23		209.2	210.4	208.6	209.4
24		159.0	160.8	158.2	159.3
25		207.1	207.6	206.8	206.8

NO.	Treatment regions and techniques	Absolute dose at isocenter in each tube voltage (%)			
		120 kVp	DECT	80 kVp	140 kVp
26	Chest VMAT	226.5	226.8	226.4	226.5
27		245.9	247.2	245.0	246.1
28		293.6	292.1	292.2	293.2
29		206.2	206.7	205.7	206.4
30		159.0	160.6	158.8	160.2
31	Spine 3D	237.4	238.8	236.4	237.9
32		303.7	305.2	302.6	304.0
33		435.6	437.6	434.2	436.2
34		296.1	298.4	294.8	297.0
35		282.8	285.1	281.6	283.1
36	Spine IMRT	168.3	169.1	168.0	168.6
37		135.1	134.0	134.1	135.1
38		937.4	943.4	933.1	938.7
39		373.7	375.0	369.8	373.9
40		429.9	432.3	427.4	430.1
41	Spine VMAT	165.6	166.9	165.2	166.1
42		330.0	330.3	328.9	330.5
43		318.9	322.4	316.9	319.6
44		1233.7	1239.7	1229.1	1235.3
45		101.3	101.8	100.9	101.4
46	Pelvis 3D	189.4	191.1	188.3	189.8
47		172.4	174.2	171.3	172.8
48		191.0	192.5	189.5	191.3
49		180.9	182.4	179.5	181.4
50		412.9	416.8	409.7	413.7
51	Pelvis IMRT	193.4	194.9	192.3	192.2
52		209.6	211.3	208.2	209.9
53		214.5	215.9	214.2	214.7
54		184.1	186.5	182.4	184.4
55		183.4	185.2	182.1	183.9

NO.	Treatment regions and techniques	Absolute dose at isocenter in each tube voltage (%)			
		120 kVp	DECT	80 kVp	140 kVp
56	Pelvis VMAT	169.2	170.7	168.2	169.5
57		210.4	212.1	209.1	210.7
58		215.4	217.4	213.8	215.7
59		184.7	186.6	183.3	185.0
60		189.1	190.8	187.7	189.4
61	H&N+A* 3D	215.4	215.4	215.4	215.5
62		219.9	220.1	219.9	220.0
63		306.5	306.6	306.7	306.4
64		495.1	496.7	491.9	496.4
65		103.0	103.0	103.1	103.0
66	H&N+A* IMRT	180.3	180.2	179.5	180.5
67		147.3	147.5	147.5	147.4
68		207.5	207.9	205.2	207.8
69		196.2	196.4	195.0	196.5
70		226.1	226.4	225.4	226.4
71	H&N+A* VMAT	200.4	200.7	199.7	200.6
72		193.5	193.8	192.5	193.9
73		149.4	149.6	149.1	149.3
74		214.6	215.0	213.4	215.0
75		197.3	197.5	196.1	197.2

VITA

NAME	Miss Siriporn Wong
SEX	Female
NATIONALITY	Thai
DATE OF BIRTH	4 January 1992
PLACE OF BIRTH	Trang
INSTITUTIONS ATTENDED	Mahidol University, 2013: Bachelor of Science (Radiological Technology)
ADDRESS	61/49 Moo 3 Tambon. Makamtie Amphoe. Meuang Suratthani 84000 Tel. 0898714123